iScience

CellPress
OPEN ACCESS

Article

Markovnikov alcohols via epoxide hydroboration by molecular alkali metal catalysts

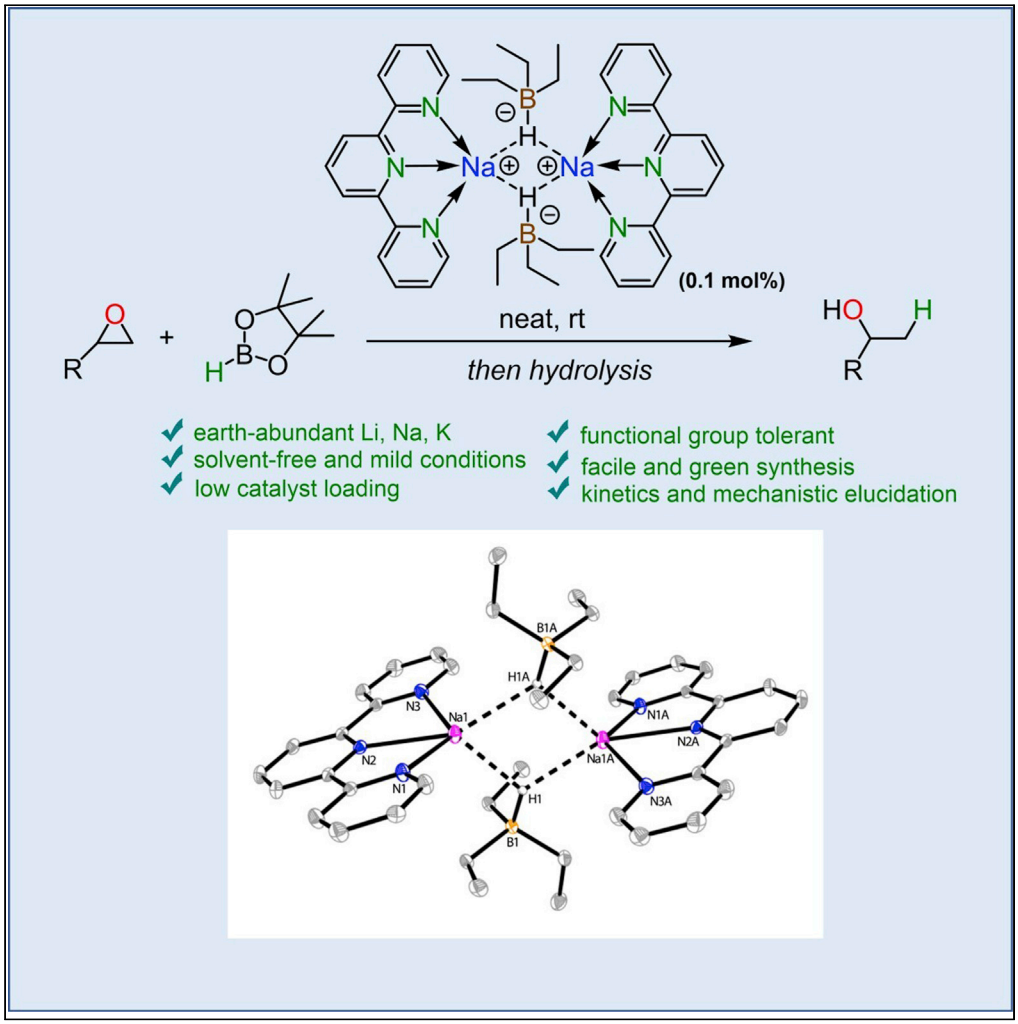

Guoqi Zhang, Haisu Zeng, Shengping Zheng, Michelle C. Neary, Pavel A. Dub

guzhang@jjay.cuny.edu (G.Z.)
pavel.dub@schrodinger.com (P.A.D.)

Highlights

A catalytic protocol for regioselective epoxide ring-opening

Well-defined alkali metal molecular catalysts based on metal triethylborohydrides

Reduction of optically active epoxides without loss of optical purities

Mechanistic studies through computational results and kinetic data

Zhang et al., iScience 25, 105119
October 21, 2022
https://doi.org/10.1016/j.isci.2022.105119

iScience

CellPress
OPEN ACCESS

Article

Markovnikov alcohols via epoxide hydroboration by molecular alkali metal catalysts

Guoqi Zhang,[1,5,*] Haisu Zeng,[1,2] Shengping Zheng,[2] Michelle C. Neary,[2] and Pavel A. Dub[3,4,*]

SUMMARY

Synthesis of branched "Markovnikov" alcohols is crucial to various chemical industries. The catalytic reduction of substituted epoxides under mild conditions is a highly attractive method for preparing such alcohols. Classical methods based on heterogeneous or homogeneous transition metal-catalyzed hydrogenation, hydroboration, or hydrosilylation usually suffer from poor selectivity, reverse regioselectivity, limited functional group compatibility, high cost, and/or low availability of the catalysts. Here we report the discovery of highly regioselective hydroboration of nonsymmetrical epoxides catalyzed by ligated archetypal reductants in organic chemistry – alkali metal triethylborohydrides. The chemoselectivity and turnover efficiencies of the present catalytic approach are excellent. Thus, terminal and internal epoxides with ene, yne, aryl, and halo groups were selectively and quantitatively reduced under a substrate-to-catalyst ratio (S/C) of up to 1000. Mechanistic investigations point to a mechanism reminiscent of frustrated Lewis pair action on substrates in which a nucleophile and Lewis acid act cooperatively on the substrate.

INTRODUCTION

Markovnikov alcohols are important chemicals with myriad applications in bulk/fine agrochemicals, pharmaceuticals, and fragrance industries. Thus, their synthesis is continuous of great interest. Petroleum-derived olefins are currently the largest-volume building blocks to access alcohol. Mono- or polysubstituted olefins can give two regioisomeric alcohols in the general case (Yao et al., 2019; Dong et al., 2011; Jensen and Trogler, 1986). Markovnikov alcohols, in which the hydroxyl group is bound to the more substituted one of the two adjacent carbons (Figure 1), can be obtained from such olefins by liquid or solid acid catalyzed hydration or a two-step Wacker oxidation-reduction process. However, owing to the frequent limitations of these transformations (isomerization, cyclization, poor catalyst performance, equilibria issues and/or harsh conditions employed, limited functional group tolerance, chemoselectivity), stoichiometric oxymercuration-demercuration (Brown and Geoghegan, 1967), catalytic Mukaiyama hydration (Shigeru and Teruaki, 1989) as well as enzymatic hydration (Demming et al., 2019) reactions emerged as more efficient methods (Figure 1).

The reduction of strained epoxides, easily obtainable from olefins via epoxidation, is an alternative method of preparing alcohols (Yao et al., 2019). The combination of appropriately regioselective and functional-group-tolerant reduction with the inexpensive and selective epoxidation of olefins will permit the two-step synthesis of functionalized alcohols. Conventional methods for epoxide ring-opening are based on stoichiometric amounts of strong reducing agents such as $LiAlH_4$. Such methods usually suffer from poor regioselectivities by providing a mixture of both primary and secondary alcohols, poor functional group tolerance, and the generation of enormous amounts of waste. Heterogeneous (Duval et al., 2021; Thiery et al., 2007; Nandi et al., 2017) and particularly homogeneous transition-metal catalyzed hydrogenation (Yao et al., 2019; Liu et al., 2019), hydroboration (Patnaik and Sadow, 2019; Song et al., 2017; Desnoyer et al., 2017), and hydrosilylation (Zhang et al., 2017, 2018; Wenz et al., 2017; Henriques et al., 2016; Gansäuer et al., 2012; Park and Brookhart, 2011; Nagashima et al., 2000) of epoxides as well as transition-metal-free approaches (Patnaik and Sadow, 2019; Zhang et al., 2018; Huang et al., 2022; Ton et al., 2021) were developed by several laboratories leading preferentially to *anti*-Markovnikov alcohols. Many fewer catalysts have been reported for the selective reduction of epoxides into Markovnikov alcohols. Examples include heterogeneous (Kwon et al., 2007) and homogeneous hydrogenation (Thiyagarajan and Gunanathan, 2019; Ito et al., 2003; Fujitsu et al., 1981) as well as transfer hydrogenation (Oshima et al., 1989)

[1]Department of Sciences, John Jay College and PhD in Chemistry Program, the Graduate Center of City University of New York, New York, NY 10019, USA

[2]Department of Chemistry, Hunter College, City University of New York, New York, NY 10065, USA

[3]Chemistry Division, Los Alamos National Laboratory, Los Alamos, NM 87545, USA

[4]Present address: Schrödinger Inc., San Diego, California 92121, United States

[5]Lead contact

*Correspondence: guzhang@jjay.cuny.edu (G.Z.), pavel.dub@schrodinger.com (P.A.D.)

https://doi.org/10.1016/j.isci.2022.105119

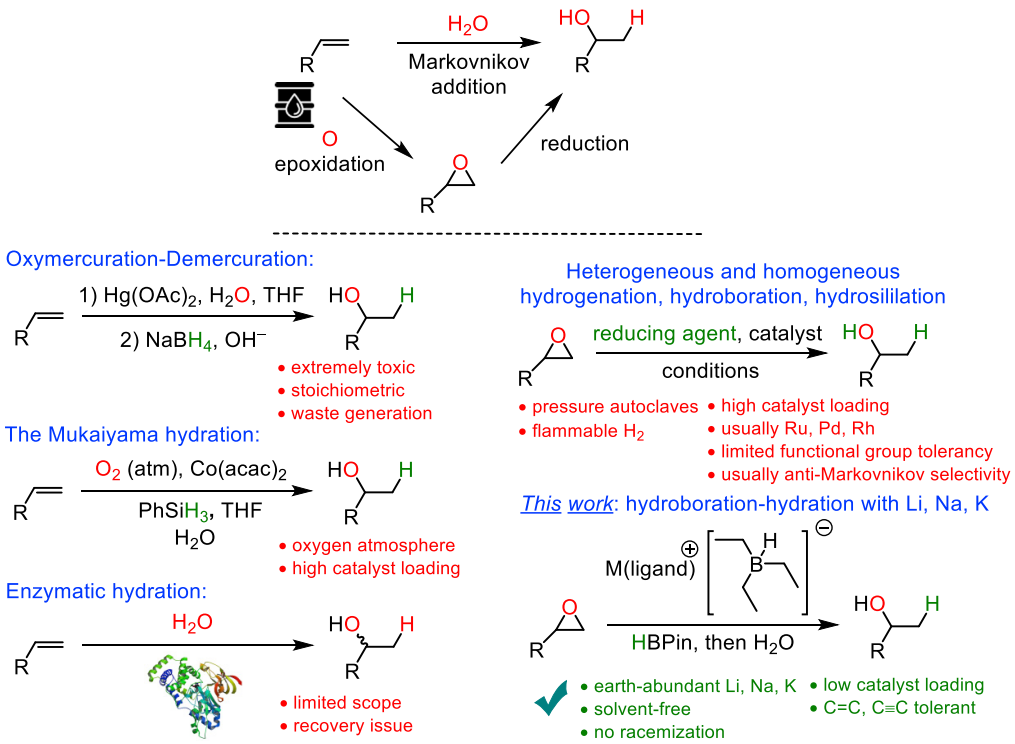

Figure 1. Current state-of-the-art in regioselective approaches to Markovnikov alcohols and the new method developed in this work. M = Li, Na, K

with precious metals (Ru, Rh, Pd), substrate limited hydrosilylation with Zn (Mimoun, 1999), and high-catalyst loading hydroboration with alkaline-earth Mg (Magre et al., 2022; Cao et al., 2020). Noyori-type molecular catalysts based on precious Ru (Thiyagarajan and Gunanathan, 2019; Ito et al., 2003) are particularly regio- and/or chemoselective methods, but are either limited to terminal epoxides (Thiyagarajan and Gunanathan, 2019; Ito et al., 2003) or monosubstituted epoxides (Ito et al., 2003), and/or are not tolerant to terminal C=C bonds (Thiyagarajan and Gunanathan, 2019). Selective reduction of unsymmetrical epoxides bearing terminal and internal double bonds leading to olefinic Markovnikov alcohols would be of particular value (Ibrahim et al., 2017).

Here we report an example of highly selective epoxide ring-opening catalyzed by major rock-forming non-transition metal-based species, being some of the most abundant metals in the Earth's crust (M = Li, Na, and K). *s*-Block metal catalysis is an active field of study (Magre et al., 2022). However, the potential of such catalysts is still underexplored relative to *d*-block catalysts. We found that readily available and inexpensive off-the-shelf alkali metal triethylborohydrides in the presence of a ligand catalyze highly regio- and chemoselective hydroboration of substituted epoxides producing secondary alcohols in excellent yields and with broad functional group tolerance.

RESULTS AND DISCUSSION

Inspired by the recently discovered catalytic activity of traditional reducing agent $LiAlH_4$ (Elsen et al., 2018), we attempted to reduce model substrate styrene oxide **8a** by pinacolborane (HBpin) with a catalytic amount of $LiAlH_4$ along with more common $NaBH_4$, KBH_4 and BH_3-THF reagents under neat conditions (Scheme S1). In all cases negligible (~20) turnovers were detected. The existence of catalytic activity for $NaBH_4$ supplements the previously reported data on anti-Markovnikov BH_3 addition (Brown and Yoon, 1968), although the regioselectivity was not measured in our case owing to the poor yield. Furthermore, similarly, poor activity was found for corresponding saline MH (M = Li, Na, K) hydrides (Scheme S1). Promisingly, we found that stronger reducing agents such as $MHBEt_3$ (M = Li, Na, K; Et = ethyl) are one-order more efficient for the same reaction, leading to an appreciable ~500 turnovers (Scheme S1). Moreover, consistent with the stoichiometric reduction of epoxides with these reagents, the regioselectivity of ~9:1

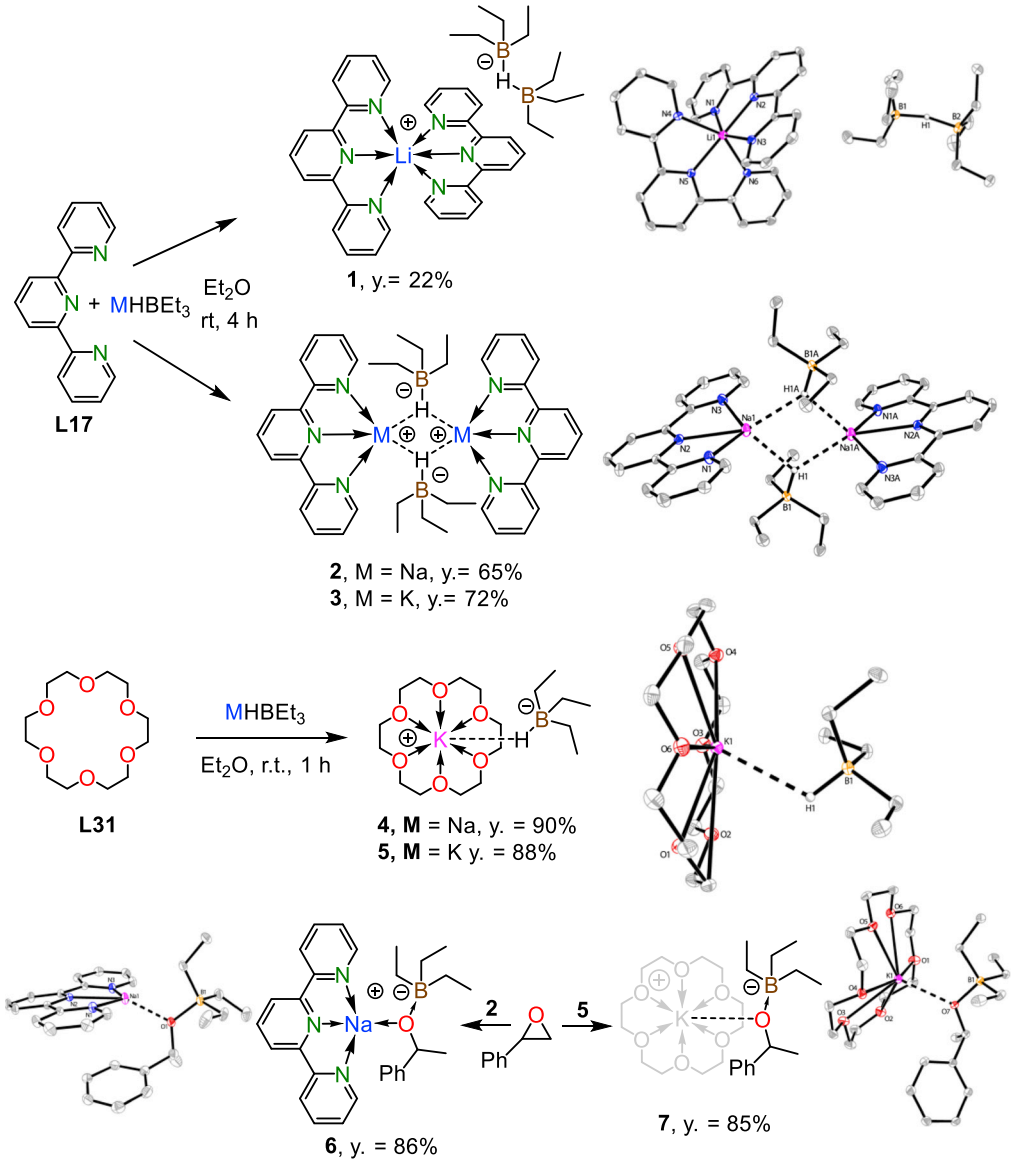

Figure 2. Synthesis of complexes 1-7 including the isolation of active catalytic species and possible reaction intermediates through stoichiometric reactions

X-ray structures are drawn with ellipsoids at a 30% probability level. Non-critical H-atoms are omitted. The X-ray structure of **3** is isostructural to **2**. See also Figures S1–S6, and Table S1.

was noted in favor of the Markovnikov product. Inspired by this notable activity and promising selectivity, we further tested the same reactions in the presence of 1 equiv of various commercially available mono- and polydentate organic ligands (Scheme S2). Based on 102 tested reactions, a ligand was found to generally have a beneficial effect on both the catalytic efficiency and regioselectivity. For example, the reaction yield increased to ~99% from an average of 40%, whereas the regioselectivity reached up to a ~40:1 ratio in the best cases.

In the next step, by using two promising ligands for both efficiency and selectivity, namely 2,2′:6′,2″-terpyridine (**L17**) and 18-crown-6 (**L31**), we attempted to isolate active catalytic species and reaction intermediates. For M/**L17** (M = Li, Na, and K) and M/**L31** (M = Na and K), isolable complexes **1**-**5** were obtained in moderate-to-appreciable yields and characterized by NMR spectroscopies and X-ray crystallography (Figure 2 and supplemantary information). The stoichiometric reaction of styrene oxide with

isolated **2** and **5** afforded products **6** and **7**, respectively, the regioselectivity of which is consistent with the Markovnikov formulation.

Notably, all the isolable complexes **1**-**7** are active catalyst precursors for the hydroboration of styrene oxide (Scheme S3). Furthermore, complexes **1**-**7** feature even improved activity and/or selectivity relevant to the *in situ* 1:1 M[$HBEt_3$]/ligand reactivity (Schemes S2 and S3). We particularly noted 30:1 Markovnikov selectivity achieved with complexes **2** or **3** in the quantitative (>99%) hydroboration of styrene oxide under neat conditions (Scheme S3). Next, we compared the efficiency of **1**-**7** with various homogeneous catalysts from our laboratories, popular commercially available metal−ligand bifunctional catalysts, classical precious metal catalyst precursors, as well as $MgBu_2$ being the state-of-the-art catalyst for Markovnikov epoxide hydroboration (Magre et al., 2020) (Scheme S3). Under identical conditions employed, all the complexes based on transition metals screened were found to be very poor catalysts. Furthermore, all complexes **1**-**7** provide significantly higher activity and selectivity for this reaction relative to $MgBu_2$, placing them to the category of most-efficient catalysts reported to date for the reaction under study.

In the next step, after proper optimization of the reaction conditions as summarized in Table S2, we tested the scope for the hydroboration of various simple and functional epoxides **8** catalyzed by **2** under solvent-free conditions (Figure 3).

We found that epoxides **8** were quantitatively reduced in the presence of such reducible groups as terminal and internal ene, yne, aryl, and halo by using only 0.1 mol % catalyst loading, and the corresponding secondary alcohols **9** were isolated in good to high yields after hydrolysis. We also noted that the regioselectivity remains on a very high level (25:1 to 99:1) for all substrates tested except 4-fluorostyrene oxide which affords the Markovnikov alcohol with 12:1 regioselectivity. The potential application of our catalyst in the industrial synthesis of Markovnikov alcohols was demonstrated in the example of **8f** hydroboration performed at a 10 mmol scale (see Scheme S4). Thus, 1.34 g of the corresponding product **9f** was isolated in 88% yield from the reaction where only 5.4 mg of catalyst **2** was used (S/C = 1000). Similarly to $MgBu_2$ (Magre et al., 2020), catalyst **2** also promoted the ring opening of less-reactive oxetane by hydroboration with good yield, yet it showed no activity toward the much more challenging oxolane from our preliminary catalytic test (Scheme S5). Limitations of our method have been noticed for several functionalized oxiranes that contain ester, sulfonate, and N-heterocyclic groups (Scheme S6). In addition, the carbonyl-containing oxirane, 1,3-diphenyl-2,3-epoxy-1-propanone was found to be selectively hydroborated on the ketone over the oxirane with high yield (Figure S7). Pleasingly, when enantioenriched (*S*)-**8a** was employed for the hydroboration catalyzed by **2**, no detectable loss of enantiomeric excess was observed (Scheme S7).

Next, we performed a deuterium-labeling experiment, kinetics studies, and computational analysis based on Density Functional Theory (DFT) aimed at building the mechanistic understanding of **2**-catalyzed hydroboration. Here, our goal was to decipher the role that the sodium cation, the anion, and the **L17** ligand alone and altogether played in the catalytic reaction. A further goal was to identify the regioselectivity-determining step and probe the identity of the catalytic cycle. Full details are available in the supplemantary information, and here we would like to summarize the most important findings.

Hydroboration of styrene oxide with DBpin shows >50:1 Markovnikov selectivity with deuterium atom incorporation at the less-substituted methylene group. The regioselectivity thus nearly doubled relative to HBpin, where a 30:1 ratio was observed. The corresponding product $PhCH(OH)CH_2D$ was isolated in 90% yield (Scheme S9). The initial rates method indicates that the catalytic reaction displays first-order dependence on both styrene oxide and HBpin concentrations and one-half order in **2** concentration leading to approximately the following rate equation in tetrahydrofuran: $d[product]/dt \sim k[\text{styrene oxide}]^1[HBpin]^1[\mathbf{2}]^{0.5}$ with $k \approx 0.39\ min^{-1}\ M^{-1.5}$ at 25°C, see supplemantary information. Kinetic studies thus indicate that both styrene oxide and HBpin enter the rate-determining zone of the catalytic cycle as well as corroborate the mononuclear reactivity of **2**, which therefore dissociates into two fragments under catalytic conditions.

To uncover the role that the sodium cation, the $[HBEt_3]^-$ anion, and the **L17** ligand play in the regioselectivity-determining step, we have chosen the substrate **8f** that affords the product **9f** with the appreciably high regioselectivity of >99% in the computational analysis. Various transition states were manually sampled based on plausible bimolecular and trimolecular combinations (see STAR Method and supplemantary information). The optimized geometries of the most energetically accessible transition states are shown in Figure 4A.

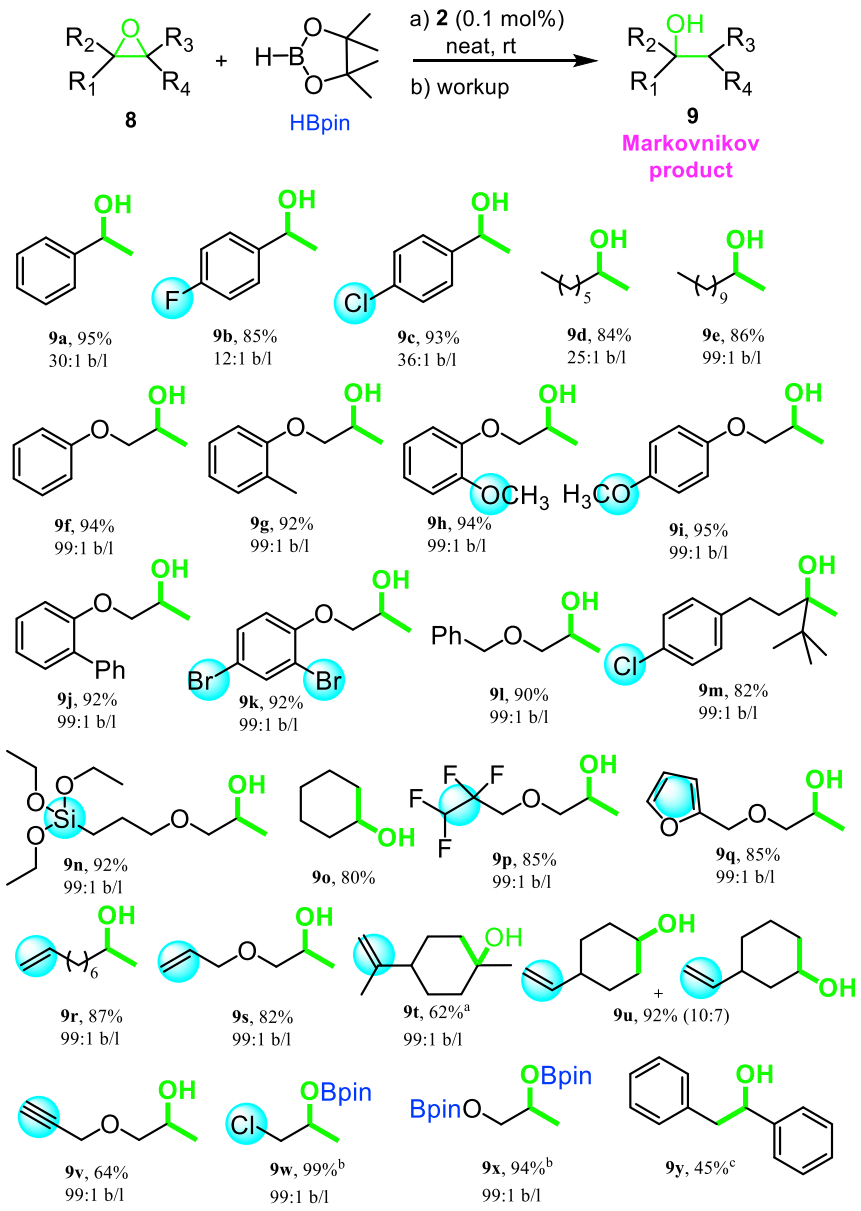

Figure 3. The substrate scope for 2-catalyzed hydroboration of epoxides

Conditions: epoxides (1.0 mmol), pinacolborane (1.1 mmol) and **2** (S/C = 1000), neat, rt, N_2, 2 h (to ensure the completion of reactions). Complete conversion unless otherwise described. Isolated yields and ratios of two regioisomers determined by GC analysis using hexamethylbenzene as an internal standard.

[a]Reaction run in THF (1 mL) for 16 h, 75% conversion.

[b]NMR yield with hexamethylbenzene as an internal standard.

[c]Reaction run in THF (1 mL) at 80°C for 16 h, 55% conversion. See also Schemes S1–S9, Figure S7, and Table S2.

Computations predict the highest regioselectivities for naked $[HBEt_3]^-$ based on a computed 5.5 kcal mol^{-1} energy gap between the transition states leading to Markovnikov (TS_A) and *anti*-Markovnikov (TS_D) products. The addition of sodium to the model leads to a change in the molecularity (bimolecular → trimolecular) and a decrease in the energy gap to 2.6 kcal mol^{-1} between the Markovnikov (TS_H) and *anti*-Markovnikov (TS_K) transition states. Thus, the presence of the cation in a non-covalent bonding position near the epoxide oxygen atom in the transition states decreases the Markovnikov regioselectivity. In the full reaction mixture, there are various states possible corresponding to tight $[HBEt_3]^-Na^+$, various solvent-shared/solvent-separated ion pairs, and free ions. Each of these species would ultimately contribute

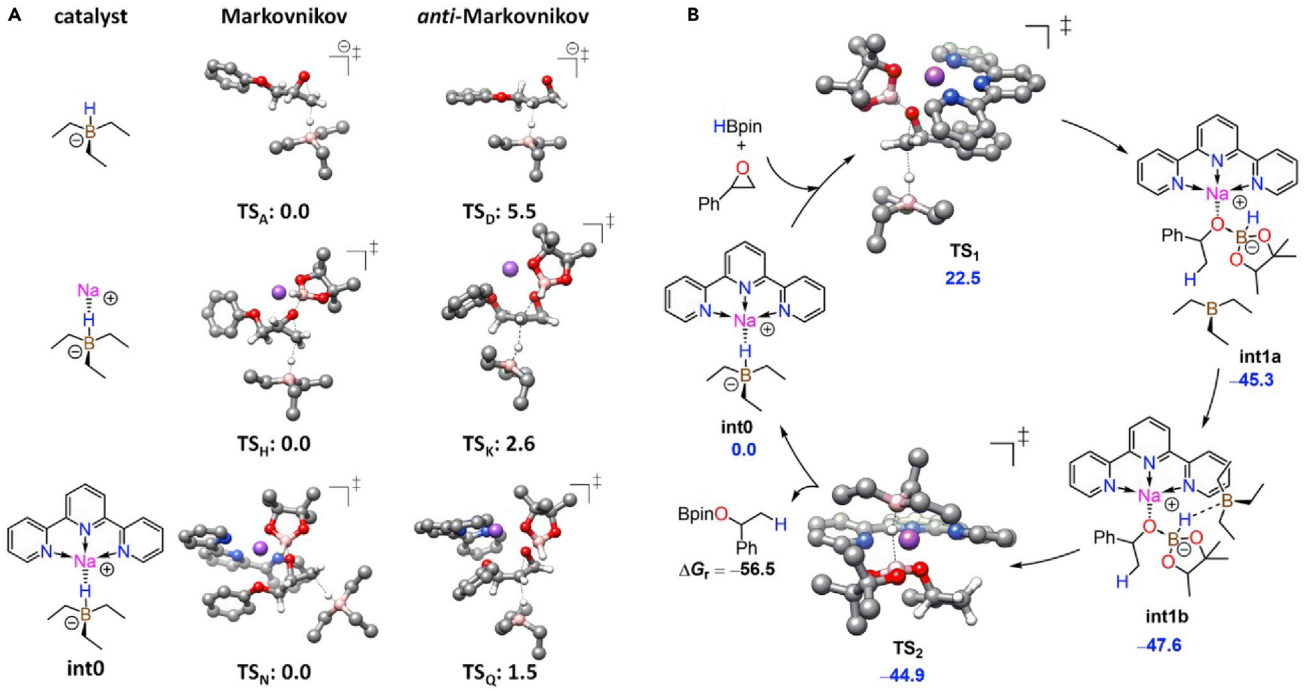

Figure 4. Mechanistic studies

(A) Geometries of optimized transition states determining Markovnikov vs *anti*-Markovnikov selectivities in the hydroboration of **8f** based on $[HBEt_3]^-$, $[HBEt_3]^-Na^+$ and $[HBEt_3]^-Na^+$(**L17**) species.

(B) Catalytic cycle for **8a** hydroboration catalyzed by **2**, suggested by combined computational analysis and kinetics data. Non-critical H-atoms and all non-covalent interactions with Na are omitted for clarity for the optimized transition state structures, and dashed bonds represent transition vectors.

All relative standard free energies are reported in kcal•mol^{-1}. See also Figures S8–S13 and Tables S3–S6.

to the final regioselectivity, so the computed transition state energy gap for the reaction with $[HBEt_3]^-Na^+$ is, therefore, expected to lie between 2.6 and 5.5 kcal/mol. Because the experimental regioselectivity is small (12:1, which represents a relatively small 1.5 kcal/mol delta for the barrier at RT = 0.59 kcal/mol, see Scheme S8), the most populated species is likely to be a tight $[HBEt_3]^-Na^+$ ion pair. The discrepancy between the experimental 1.5 kcal/mol and the computed 2.6-5.5 kcal/mol range is possible owing to the limitations of the computational approach and/or experimental issues, e.g. potential background reactions that could lower selectivity. Nevertheless, the discrepancy is computationally small and these computational results provide a reasonable rationalization for the experimental observations with $[HBEt_3]^-Na^+$.

The experimental reaction of **8f** with precatalyst **2**, however, provides better regioselectivity (99:1, which represents a 2.7 kcal/mol delta for the barrier). One might anticipate that the ligand **L17** either decreases the Lewis acidity of the cation and/or shifts the equilibrium in the ensemble toward free ions. Though full ion separation is the ideal case from a regioselectivity standpoint according to the calculations, this does not appear to be the case under the experimental catalytic conditions. Catalytic reactions of similar model compound **8a** with $[HBEt_3]^-Na^+$ in the presence of 0, 1, or 2 equiv of **L17** all showed comparable regioselectivity (9:1, 10:1, and 9:1, respectively), although with varying yields (Schemes S1 and S2). Furthermore, precatalyst **1**, a six-coordinate bisligated-monometal complex, shows comparable regioselectivity relative to monoligated catalyst precursors (Scheme S3), which suggests its transformation into the monoligated species under catalytic conditions.

The computational analysis of the transition states TS_N–TS_Q for $[HBEt_3]^-Na$(**L17**)$^+$ (**int0**) (Figure 4A) does, indeed, reproduce the observed Markovnikov regioselectivity for the reaction of **8f** with **2**. However, the computed energy gap of 1.5 kcal mol^{-1} is below the 2.6-5.5 kcal/mol range computed for $[HBEt_3]^-Na^+$ and $[HBEt_3]^-$ alone, despite the experimental reaction with **2** being more regioselective than that with $[HBEt_3]^-Na^+$. The computed gap is also slightly below the experimentally determined 2.7 kcal/mol. Most likely, this is a virtual result owing to an incomplete conformational sampling achieved

in our calculations, or owing to the computational accuracy of the DFT method being ±3 kcal/mol, see supplemantary information. It is also possible that we have not properly identified the mechanism of regioselectivity and/or the catalytic reaction. However, the experimental and kinetics data do support the proposed rate-determining intermediate, and the computational analysis of this mechanism does support the Markovnikov regioselectivity overall. Thus, we conclude based on combined experimental observations, kinetics data, and computational data for $[HBEt_3]^-Na^+$ that the monoligated and monometal tight ion-pair complex $[HBEt_3]^-Na(\mathbf{L17})^+$ (**int0**) is the likely catalytic species.

The full proposed computed catalytic cycle for the hydroboration of related test styrene oxide **8a** with **2** is displayed in Figure 4B (see STAR Method and supplemantary information for more details including further explanation of how we ruled out other possible reaction pathways). Here, species **int0** serves as the catalyst and selectivity-determining intermediate, and $\mathbf{TS_1}$, representing the concerted epoxide ring-opening by the $[HBEt_3]^-$ anion and HBpin, serves as the rate- and selectivity-determining transition state. The identity of these determining states is consistent with the experimental rate law, which is half-order in **2**, and first-order in both HBpin and **8a**. The computed energetic span of the overall reaction is 22.5 kcal/mol, a reasonable value for an S/C of 1000 and quantitative conversion under ambient conditions. Clearly, the monoligated alkali metal cation plays an important role within the catalytic cycle to establish a three-dimensional molecular assembly stabilized by non-covalent interactions.

Conclusions

In summary, we report a convenient catalytic protocol for the synthesis of Markovnikov alcohols via hydroboration of epoxides in the presence of old and cheap "stoichiometric" reagents $MHBEt_3$ (M = Li, Na, K) which become efficient catalysts upon coordination with various chelating ligands such as terpyridine or crown ethers. The method is tolerant to various functional and stereo groups and also reduces optically active expoxides without loss of optical purities, which further adds value to the present catalytic system. Computational analysis and kinetic studies indicate that both the $[HBEt_3]^-$ anion and alkali metal cation are equally important for catalytic activity. The former determines catalytic efficiency, whereas the latter controls the reaction selectivity. Analysis of the catalytic cycle indicates that both the rate- and regioselectivity-determining transition state of this reaction is concerted HBpin-assisted epoxide ring-opening by the $[HBEt_3]^-$ anion. The ligated alkali metal cation plays an important role within the catalytic cycle to establish a three-dimensional molecular assembly stabilized by non-covalent interactions. This is somewhat reminiscent of the concept of Stephan's frustrated Lewis pairs (Stephan, 2015).

Limitations of the study

This work reports a highly efficient and regioselective method for the preparation of Markovnikov alcohols via hydroboration of epoxides using well-defined alkali metal complexes of terpyridine or crown ethers. Although a good substrate scope of epoxides has been demonstrated, this method shows limitations on more challenging substrates such as oxolanes and complex oxiranes containing other reducible groups such as ketone, N-heterocycle, nitro, and ester (Schemes S5, S6 and Figure S7). Further optimization of catalysts and reaction conditions is needed to expand the scope of substrates and improve the applicability of the method.

STAR★METHODS

Detailed methods are provided in the online version of this paper and include the following:

- KEY RESOURCES TABLE
- RESOURCE AVAILABILITY
  - Lead contact
  - Materials availability
  - Data and code availability
- METHOD DETAILS
  - General information

SUPPLEMENTAL INFORMATION

Supplemental information can be found online at https://doi.org/10.1016/j.isci.2022.105119.

ACKNOWLEDGMENTS

We are grateful for the funding support by the National Science Foundation for this work (CHE-1900500). We also acknowledge the PSC-CUNY awards (63809-0051, 64254-0052, and 65203-0053) from the City University of New York. A COVID Recovery Kickstart Grant from John Jay College is gratefully acknowledged. Partial support Los Alamos National Laboratory (LANL) Directed Research and Development Program is acknowledged. Computations were performed by using Darwin Computational Cluster at LANL. This material is also based upon work supported by the Air Force Office of Scientific Research under award number FA9550-20-1-0158.

AUTHOR CONTRIBUTIONS

G.Z., H.Z., and P.A.D. performed the experimental and mechanistic studies. M.C.N. conducted the X-ray crystallographic analysis. P.A.D. designed and performed the computational studies. G.Z., S.Z., and P.A.D. conceived and supervised the project. All authors analyzed the data and wrote the article.

DECLARATION OF INTERESTS

The authors declare no competing interests.

Received: June 1, 2022
Revised: August 29, 2022
Accepted: September 8, 2022
Published: October 21, 2022

REFERENCES

Blum, Y., Czarkie, D., Rahamim, Y., and Shvo, Y. (1985). Cyclopentadienone)ruthenium carbonyl complexes - a new class of homogeneous hydrogenation catalysts. Organometallics *4*, 1459–1461. https://doi.org/10.1021/om00127a027.

Brown, H.C., and Geoghegan, P. (1967). The oxymercuration-demercuration of representative olefins. A convenient, mild procedure for the Markovnikov hydration of the carbon-carbon double bond. J. Am. Chem. Soc. *89*, 1522–1524. https://doi.org/10.1021/ja00982a043.

Brown, H.C., and Yoon, N.M. (1968). The borohydride-catalyzed reaction of diborane with epoxides. The anti- Markovnikov opening of trisubstituted epoxides. J. Am. Chem. Soc. *90*, 2686–2688. https://doi.org/10.1021/ja01012a039.

Cao, X., Li, J., Zhu, A., Su, F., Yao, W., Xue, F., and Ma, M. (2020). Syntheses of asymmetrical magnesium(i) complexes and their catalytic application in epoxide hydroboration. Org. Chem. Front. *7*, 3625–3632. https://doi.org/10.1039/D0QO00938E.

Castro, P.M., Lahtinen, P., Axenov, K., Viidanoja, J., Kotiaho, T., Leskelä, M., and Repo, T. (2005). Activation of 2, 6-Bis(imino)pyridine iron(II) chloride complexes by methylaluminoxane: an electrospray ionization tandem mass spectrometry investigation. Organometallics *24*, 3664–3670. https://doi.org/10.1021/om050351s.

Chai, J.-D., and Head-Gordon, M. (2008). Long-range corrected hybrid density functionals with damped atom–atom dispersion corrections. Phys. Chem. Chem. Phys. *10*, 6615–6620. https://doi.org/10.1039/B810189B.

Crockett, M.P., Wong, A.S., Li, B., and Byers, J.A. (2020). Rational design of an iron-based catalyst for Suzuki–Miyaura cross-couplings involving heteroaromatic boronic esters and tertiary alkyl electrophiles. Angew. Chem. Int. Ed. Engl. *59*, 5392–5397. https://doi.org/10.1002/anie.201914315.

Demming, R.M., Hammer, S.C., Nestl, B.M., Gergel, S., Fademrecht, S., Pleiss, J., and Hauer, B. (2019). Asymmetric enzymatic hydration of unactivated, aliphatic alkenes. Angew. Chem. Int. Ed. Engl. *58*, 173–177. https://doi.org/10.1002/anie.201810005.

Desnoyer, A.N., Geng, J., Drover, M.W., Patrick, B.O., and Love, J.A. (2017). Catalytic functionalization of styrenyl epoxides via 2-nickela(II)oxetanes. Chemistry *23*, 11509–11512. https://doi.org/10.1002/chem.201702824.

Dong, G., Teo, P., Wickens, Z.K., and Grubbs, R.H. (2011). Primary alcohols from terminal olefins: formal anti- Markovnikov hydration via triple relay catalysis. Science *333*, 1609–1612. https://doi.org/10.1126/science.aaw3913.

Dong, Y., Fan, R., Wang, X., Wang, P., Zhang, H., Wei, L., Song, Y., Du, X., Chen, W., and Yang, Y. (2016). Topological evolution in mercury(II) Schiff base complexes tuned through alkyl substitution – synthesis, solid-state structures, and aggregation-induced emission properties. Eur. J. Inorg. Chem. *2016*, 3598–3610. https://doi.org/10.1002/ejic.201600231.

Dub, P.A., and Gordon, J.C. (2017). Metal–ligand bifunctional catalysis: the "accepted" mechanism, the issue of concertedness, and the function of the ligand in catalytic cycles involving hydrogen atoms. ACS Catal. *7*, 6635–6655. https://doi.org/10.1021/acscatal.7b01791.

Dub, P.A., Scott, B.L., and Gordon, J.C. (2015). Air-stable NNS (ENENES) ligands and their well-defined ruthenium and iridium complexes for molecular catalysis. Organometallics *34*, 4464–4479. https://doi.org/10.1021/acs.organomet.5b00432.

Duval, M., Deboos, V., Hallonet, A., Sagorin, G., Denicourt-Nowicki, A., and Roucoux, A. (2021). Selective palladium nanoparticles-catalyzed hydrogenolysis of industrially targeted epoxides in water. J. Catal. *396*, 261–268. https://doi.org/10.1016/j.jcat.2021.02.027.

Ebralidze, I.I., Leitus, G., Shimon, L.J., Wang, Y., Shaik, S., and Neumann, R. (2009). Structural variability in manganese(II) complexes of N, N′-bis(2-pyridinylmethylene) ethane (and propane) diamine ligands. Inorganica Chim. Acta *362*, 4713–4720. https://doi.org/10.1016/j.ica.2009.06.037.

Elsen, H., Färber, C., Ballmann, G., and Harder, S. (2018). $LiAlH_4$: from stoichiometric reduction to imine hydrogenation catalysis. Angew. Chem. Int. Ed. *57*, 7156–7160. https://doi.org/10.1002/anie.201803804.

Frisch, M.J., Trucks, G.W., Schlegel, H.B., Scuseria, G.E., Robb, M.A., Cheeseman, J.R., Scalmani, G., Barone, V., Petersson, G.A, and Nakatsuji, H. et al. (2016). Gaussian 16, Revision C.01. Gaussian Inc.

Fujitsu, H., Shirahama, S., Matsumura, E., Takeshita, K., and Mochida, I. (1981). Catalytic hydrogenation of styrene oxide with cationic rhodium complexes. J. Org. Chem. *46*, 2287–2290. https://doi.org/10.1021/jo00324a016.

Gansäuer, A., Klatte, M., Brändle, G.M., and Friedrich, J. (2012). Catalytic hydrogen atom transfer (HAT) for sustainable and diastereoselective radical reduction. Angew. Chem. Int. Ed. Engl. *51*, 8891–8894. https://doi.org/10.1002/anie.201202818.

Grimme, S. (2006). Semiempirical GGA-type density functional constructed with a long-range dispersion correction. J. Comput. Chem. *27*, 1787–1799. https://doi.org/10.1002/jcc.20495.

Hadlington, T.J., Hermann, M., Frenking, G., and Jones, C. (2014). Low coordinate germanium(II) and tin(II) hydride complexes: efficient catalysts for the hydroboration of carbonyl compounds. J. Am. Chem. Soc. *136*, 3028–3031. https://doi.org/10.1021/ja5006477.

Henriques, D.S.G., Zimmer, K., Klare, S., Meyer, A., Rojo-Wiechel, E., Bauer, M., Sure, R., Grimme, S., Schiemann, O., Flowers, R.A., II, and Gansäuer, A. (2016). Highly active titanocene catalysts for epoxide hydrosilylation: synthesis, theory, kinetics, EPR spectroscopy. Angew. Chem. Int. Ed. *55*, 7671–7675. https://doi.org/10.1002/anie.201601242.

Huang, C., Ma, W., Zheng, X., Xu, M., Qi, X., and Lu, Q. (2022). Epoxide electroreduction. J. Am. Chem. Soc. *144*, 1389–1395. https://doi.org/10.1021/jacs.1c11791.

Hudlicky, T., Tsunoda, T., Gadamasetti, K.G., Murry, J.A., and Keck, G.E. (1991). Yeast-mediated resolution of β-keto esters of prochiral alcohols. J. Org. Chem. *56*, 3619–3623. https://doi.org/10.1021/jo00011a031.

Ibrahim, A.D., Entsminger, S.W., and Fout, A.R. (2017). Insights into a chemoselective cobalt catalyst for the hydroboration of alkenes and nitriles. ACS Catal. *7*, 3730–3734. https://doi.org/10.1021/acscatal.7b00362.

Ito, M., Hirakawa, M., Osaku, A., and Ikariya, T. (2003). Highly efficient chemoselective hydrogenolysis of epoxides catalyzed by a (η^5-$C_5(CH_3)_5$)Ru complex bearing a 2-(diphenylphosphino)ethylamine ligand. Organometallics *22*, 4190–4192. https://doi.org/10.1021/om034006j.

Jensen, C.M., and Trogler, W.C. (1986). Catalytic hydration of terminal alkenes to primary alcohols. Science *233*, 1069–1071. https://doi.org/10.1126/science.233.4768.1069.

Kobylarski, M., Berthet, J.C., and Cantat, T. (2022). Reductive depolymerization of polyesters and polycarbonates with hydroboranes by using a lanthanum(iii) tris(amide) catalyst. Chem. Commun. *58*, 2830–2833. https://doi.org/10.1039/D2CC00184E.

Kozuch, S., Lee, S.E., and Shaik, S. (2009). Theoretical analysis of the catalytic cycle of a nickel cross-coupling process: application of the energetic span model. Organometallics *28*, 1303–1308. https://doi.org/10.1021/om800772g.

Kumar, R.N., Chauhan, N.K., Das, A.K., and Singh, S.K. (2001). Synthesis and characterization of Pd(II) and Pt(II) complexes of 2-pyridyl methyl ketazine. Asia. J. Chem. *13*, 752–754.

Kuriyama, W., Matsumoto, T., Ogata, O., Ino, Y., Aoki, K., Tanaka, S., Ishida, K., Kobayashi, T., Sayo, N., and Saito, T. (2012). Catalytic hydrogenation of esters. Development of an efficient catalyst and processes for synthesising (R)-1, 2-propanediol and 2-(l-menthoxy)ethanol. Org. Process Res. Dev. *16*, 166–171. https://doi.org/10.1021/op200234j.

Kwon, M.S., Park, I.S., Jang, J.S., Lee, J.S., and Park, J. (2007). Magnetically separable Pd catalyst for highly selective epoxide hydrogenolysis under mild conditions. Org. Lett. *9*, 3417–3419. https://doi.org/10.1021/ol701456w.

Liu, W., Li, W., Spannenberg, A., Junge, K., and Beller, M. (2019). Iron-catalysed regioselective hydrogenation of terminal epoxides to alcohols under mild conditions. Nat. Catal. *2*, 523–528. https://doi.org/10.1038/s41929-019-0286-7.

Magre, M., Paffenholz, E., Maity, B., Cavallo, L., and Rueping, M. (2020). Regiodivergent hydroborative ring opening of epoxides via selective C–O bond activation. J. Am. Chem. Soc. *142*, 14286–14294. https://doi.org/10.1021/jacs.0c05917.

Magre, M., Szewczyk, M., and Rueping, M. (2022). s-Block metal catalysts for the hydroboration of unsaturated bonds. Chem. Rev. *122*, 8261–8312. https://doi.org/10.1021/acs.chemrev.1c00641.

Marenich, A.V., Cramer, C.J., and Truhlar, D.G. (2009). Universal solvation model based on solute electron density and on a continuum model of the solvent defined by the bulk dielectric constant and atomic surface tensions. J. Phys. Chem. B *113*, 6378–6396. https://doi.org/10.1021/jp810292n.

Mimoun, H. (1999). Selective reduction of carbonyl compounds by polymethylhydrosiloxane in the presence of metal hydride catalysts. J. Org. Chem. *64*, 2582–2589. https://doi.org/10.1021/jo982314z.

Molander, G.A., and McKie, J.A. (1992). Samarium(II) iodide-induced reductive cyclization of unactivated olefinic ketones. Sequential radical cyclization/intermolecular nucleophilic addition and substitution reactions. J. Org. Chem. *57*, 3132–3139. https://doi.org/10.1021/jo00037a033.

Nagashima, H., Suzuki, A., Iura, T., Ryu, K., and Matsubara, K. (2000). Stoichiometric and catalytic activation of Si−H bonds by a triruthenium carbonyl cluster, (μ^3, η^2:η^3:η^5-acenaphthylene) $Ru_3(CO)_7$: isolation of the oxidative adducts, catalytic hydrosilylation of aldehydes, ketones, and acetals, and catalytic polymerization of cyclic ethers. Organometallics *19*, 3579–3590. https://doi.org/10.1021/om0003887.

Nandi, S., Patel, P., Jakhar, A., Khan, N.H., Biradar, A.V., Kureshy, R.I., and Bajaj, H.C. (2017). Cucurbit[6]uril- stabilized palladium nanoparticles as a highly active catalyst for chemoselective hydrogenation of various reducible groups in aqueous media. ChemistrySelect *2*, 9911–9919. https://doi.org/10.1002/slct.201702196.

Oshima, M., Yamazaki, H., Shimizu, I., Nisar, M., and Tsuji, J. (1989). Palladium-catalyzed selective hydrogenolysis of alkenyloxiranes with formic acid. Stereoselectivity and synthetic utility. J. Am. Chem. Soc. *111*, 6280–6287. https://doi.org/10.1021/ja00198a045.

Park, S., and Brookhart, M. (2011). Hydrosilylation of epoxides catalyzed by a cationic η^1-silane iridium(iii) complex. Chem. Commun. *47*, 3643–3645. https://doi.org/10.1039/C0CC05714B.

Patnaik, S., and Sadow, A.D. (2019). Interconverting lanthanum hydride and borohydride catalysts for C=O reduction and C−O bond cleavage. Angew. Chem. Int. Ed. *58*, 2505–2509. https://doi.org/10.1002/anie.201813305.

Pettersen, E.F., Goddard, T.D., Huang, C.C., Couch, G.S., Greenblatt, D.M., Meng, E.C., and Ferrin, T.E. (2004). UCSF Chimera—a visualization system for exploratory research and analysis. J. Comput. Chem. *25*, 1605–1612. https://doi.org/10.1002/jcc.20084.

Sheldrick, G.M. (1981). SHELXTL, an Integrated System for Solving, Refining, and Displaying Crystal Structures from Diffraction Data (University of Göttingen).

Sheldrick, G.M. (2015). SHELXT - integrated space-group and crystal-structure determination. Acta Crystallogr. A Found. Adv. *71*, 3–8. https://doi.org/10.1107/S2053273314026370.

Shigeru, I., and Teruaki, M. (1989). A new method for preparation of alcohols from olefins with molecular oxygen and phenylsilane by the use of bis(acetylacetonato)cobalt(II). Chem. Lett. *18*, 1071–1074. https://doi.org/10.1246/cl.1989.1071.

Song, H., Ye, K., Geng, P., Han, X., Liao, R., Tung, C.-H., and Wang, W. (2017). Activation of epoxides by a cooperative iron–thiolate catalyst: intermediacy of ferrous alkoxides in catalytic hydroboration. ACS Catal. *7*, 7709–7717. https://doi.org/10.1021/acscatal.7b02527.

Steiniger, K.A., and Lambert, T.H. (2021). Primary alcohols via nickel pentacarboxycyclopentadienyl diamide catalyzed hydrosilylation of terminal epoxides. Org. Lett. *23*, 8013–8017. https://doi.org/10.1021/acs.orglett.1c03029.

Stephan, D.W. (2015). Frustrated Lewis pairs. J. Am. Chem. Soc. *137*, 10018–10032. https://doi.org/10.1021/jacs.5b06794.

Thiery, E., Le Bras, J., and Muzart, J. (2007). Palladium nanoparticles-catalyzed regio- and chemoselective hydrogenolysis of benzylic epoxides in water. Green Chem. *9*, 326–327. https://doi.org/10.1039/B616486B.

Thiyagarajan, S., and Gunanathan, C. (2019). Ruthenium-catalyzed selective hydrogenation of epoxides to secondary alcohols. Org. Lett. *21*, 9774–9778. https://doi.org/10.1021/acs.orglett.9b03995.

Ton, N.N.H., Mai, B.K., and Nguyen, T.V. (2021). Tropylium-promoted hydroboration reactions: mechanistic insights via experimental and computational studies. J. Org. Chem. *86*, 9117–9133. https://doi.org/10.1021/acs.joc.1c01208.

Vasudevan, K.V., Scott, B.L., and Hanson, S.K. (2012). Alkene hydrogenation catalyzed by nickel hydride complexes of an aliphatic PNP pincer ligand. Eur. J. Inorg. Chem. *2012*, 4898–4906. https://doi.org/10.1002/ejic.201200758.

Wenz, J., Wadepohl, H., and Gade, L.H. (2017). Regioselective hydrosilylation of epoxides catalysed by nickel(ii) hydrido complexes. Chem. Commun. *53*, 4308–4311. https://doi.org/10.1039/C7CC01655G.

Yao, C., Dahmen, T., Gansäuer, A., and Norton, J. (2019). Anti-Markovnikov alcohols via epoxide

hydrogenation through cooperative catalysis. Science *364*, 764–767. https://doi.org/10.1126/science.aaw3913.

Zhang, J., Leitus, G., Ben-David, Y., and Milstein, D. (2006). Efficient homogeneous catalytic hydrogenation of esters to alcohols. Angew. Chem. Int. Ed. Engl. *45*, 1113–1115. https://doi.org/10.1002/anie.200503771.

Zhang, G., Zeng, H., Wu, J., Yin, Z., Zheng, S., and Fettinger, J.C. (2016). Highly selective hydroboration of alkenes, ketones and aldehydes catalyzed by a well-defined manganese complex. Angew. Chem. Int. Ed. Engl. *128*, 14581–14584. https://doi.org/10.1002/ange.201607579.

Zhang, Y.-Q., Poppel, C., Panfilova, A., Bohle, F., Grimme, S., and Gansäuer, A. (2017). SN_2 reactions at tertiary carbon centers in epoxides. Angew. Chem. Int. Ed. Engl. *56*, 9719–9722. https://doi.org/10.1002/anie.201702882.

Zhang, J., Park, S., and Chang, S. (2018). Piers' borane-mediated hydrosilylation of epoxides and cyclic ethers. Chem. Commun. *54*, 7243–7246. https://doi.org/10.1039/C8CC03741H.

Zhang, G., Wu, J., Zeng, H., Neary, M.C., Devany, M., Zheng, S., and Dub, P.A. (2019a). Dearomatization and functionalization of terpyridine ligands leading to unprecedented zwitterionic Meisenheimer aluminum complexes and their use in catalytic hydroboration. ACS Catal. *9*, 874–884. https://doi.org/10.1021/acscatal.8b04096.

Zhang, G., Wu, J., Zheng, S., Neary, M.C., Mao, J., Flores, M., Trovitch, R.J., and Dub, P.A. (2019b). Redox-noninnocent ligand-supported vanadium catalysts for the chemoselective reduction of C=X (X = O, N) functionalities. J. Am. Chem. Soc. *141*, 15230–15239. https://doi.org/10.1021/jacs.9b07062.

Zhang, G., Li, S., Zeng, H., Zheng, S., and Neary, M.C. (2022). Diplumbane-catalysed solvent- and additive-free hydroboration of ketones and aldehydes. RSC Adv. *12*, 19086–19090. https://doi.org/10.1039/D2RA03731A.

STAR★METHODS

Detailed methods are provided in the online version of this paper and include the following:

KEY RESOURCES TABLE

REAGENT or RESOURCE	SOURCE	IDENTIFIER
Chemicals, peptides, and recombinant proteins		
Dibutylmagnesium, 0.5M solution in heptane	Thermo Fisher Scientific	Cat#AC377771000; CAS 1191-47-5
Tris[2-(dimethylamino)ethyl]amine	Thermo Fisher Scientific	Cat#AAH3185314; CAS 33527-91-2
Tris(2-isopropylaminoethyl)amine	Sigma-Aldrich	Cat#50-174-8595; CAS 157794-54-2
N,N,N′,N′-Tetraethyldiethylenetriamine	Sigma-Aldrich	Cat#424072-5ML; CAS 123-12-6
Bis[2-(dicyclohexylphosphino)ethyl]amine	Thermo Fisher Scientific	Cat#AAH60269MD; CAS 550373-32-5
4-Dimethylaminopyridine	Thermo Fisher Scientific	Cat#AC148270050; CAS 1122-58-3
4,4′-Dipyridyl	Thermo Fisher Scientific	Cat#AC276200050; CAS 553-26-4
2,2′-Dipyridyl	Thermo Fisher Scientific	Cat#AC117500100; CAS 366-18-7
4,5-Diazafluoren-9-one	Thermo Fisher Scientific	Cat#AAH5602803; CAS 50890-67-0
1,10-Phenanthroline	Thermo Fisher Scientific	Cat#AC157530050; CAS 66-71-7
2,9-Diphenyl-1,10-phenanthroline	Thermo Fisher Scientific	Cat#D38491G; CAS 25677-69-4
2,2′:6′,2″-Terpyridine	Thermo Fisher Scientific	Cat#AAA1775001; CAS 1148-79-4
4′-Chloro-2,2′:6′,2″-terpyridine	Thermo Fisher Scientific	Cat#AAL14728MD; CAS 128143-89-5
4′-Methoxy-2,2′:6′,2″-terpyridine	Alfa Chemistry	Cat#ACM181866502; CAS 181866-50-2
4′-Phenyl-2,2′:6′,2″-terpyridine	Sigma-Aldrich	Cat#AMBH9884D428-250MG; CAS 58345-97-4
6,6″-Dibromo-2,2′:6′,2″-terpyridine	Thermo Fisher Scientific	Cat#D5432-200MG; CAS 100366-66-3
Triphenylphosphine	Thermo Fisher Scientific	Cat#AAL0250218; CAS 603-35-0
Tricyclohexylphosphine	Thermo Fisher Scientific	Cat#AA4485403; CAS 2622-14-2
Triisopropylphosphine	Thermo Fisher Scientific	Cat#AA4168404; CAS 6476-36-4
1,1-Bis(diphenylphosphino)ferrocene	Thermo Fisher Scientific	Cat#AAB2116603; CAS 12150-46-8
Bis(diphenylphosphino)methane	Thermo Fisher Scientific	Cat#B19825G; CAS 2071-20-7
1,2-Bis(diphenylphosphino)ethane	Thermo Fisher Scientific	Cat#AAA1141906; CAS 1663-45-2
Tris[2-(diphenylphosphino)ethyl]phosphine	Thermo Fisher Scientific	Cat#AC316830010; CAS 23582-03-8
15-Crown-5	Thermo Fisher Scientific	Cat#AAA1226514; CAS 33100-27-5
18-Crown-6	Thermo Fisher Scientific	Cat#AC181560050; CAS 17455-13-9
Dibenzo-18-crown-6	Thermo Fisher Scientific	Cat#AC169800100; CAS 14187-32-7
Dibenzo-24-crown-8	Thermo Fisher Scientific	Cat#D18301G; CAS 14174-09-5
Styrene oxide	Thermo Fisher Scientific	Cat#AAL0782122; CAS 96-09-3
2-(4-Fluorophenyl)oxirane	Thermo Fisher Scientific	Cat#AAH2660006; CAS 18511-62-1
4-Chlorostyrene oxide	Thermo Fisher Scientific	Cat#AAH2651606; CAS 2788-86-5
2-Hexyloxirane	TCI America	Cat#AAB2146314; CAS 2984-50-1
1,2-Epoxydodecane	TCI America	Cat#D198425ML; CAS 2855-19-8
Phenyl glycidyl ether	Thermo Fisher Scientific	Cat#AC135350500; CAS 122-60-1
o-Cresyl glycidyl ether	Thermo Fisher Scientific	Cat#AAL1013614; CAS 2210-79-9
2-[(2-Methoxyphenoxy)methyl]oxirane	Thermo Fisher Scientific	Cat#AAH6177706; CAS 2210-74-4
4-Methoxyphenyl glycidyl ether	Thermo Fisher Scientific	Cat#AAA1978006; CAS 2211-94-1
2-[([1,1′-Biphenyl]-2-yloxy)methyl]oxirane	TCI America	Cat#B5601500G; CAS 7144-65-2
2-[(2,4-Dibromophenoxy)methyl]oxirane	TCI America	Cat#D488525G; CAS 20217-01-0

(*Continued on next page*)

Continued

REAGENT or RESOURCE	SOURCE	IDENTIFIER
Benzyl glycidyl ether	TCI America	Cat#B21085G; CAS 2930-05-4
2-[2-(4-Chlorophenyl)ethyl]-2-(1,1-dimethylethyl)oxirane	TCI America	Cat#B32905G; CAS 80443-63-6
Glycidoxypropyltrimethoxysilane	TCI America	Cat#G021025G; CAS 2530-83-8
Cyclohexene oxide	Thermo Fisher Scientific	Cat#AAA1318522; CAS 286-20-4
2-[(2,2,3,3-Tetrafluoropropoxy)methyl]oxirane	Thermo Fisher Scientific	Cat#AAH5350806; CAS 19932-26-4
2-[(2-Oxiranylmethoxy)methyl]furan	TCI America	Cat#AC348490050; CAS 5380-87-0
1,2-Epoxy-9-decene	TCI America	Cat#E04115ML; CAS 85721-25-1
Allyl glycidyl ether	Thermo Fisher Scientific	Cat#AC102941000; CAS 106-92-3
Limonene oxide	Sigma-Aldrich	Cat#218324-50G; CAS 203719-54-4
4-Vinylcyclohexene oxide	Sigma-Aldrich	Cat#152544-250ML; CAS 106-86-5
2-[(2-Propyn-1-yloxy)methyl]oxirane	TCI America	Cat#G04451G; CAS 18180-30-8
Epichlorohydrin	Thermo Fisher Scientific	Cat#AC117780250; CAS 106-89-8
Glycidaldehyde	Sigma-Aldrich	Cat#ENAH03855F9A-50MG; CAS 765-34-4
trans-Stilbene oxide	Thermo Fisher Scientific	Cat#AC132780250; CAS 1439-07-2
1,3-Diphenyl-2,3-epoxy-1-propanone	TCI America	Cat#D43785G; CAS 5411-12-1
Borane-tetrahydrofuran complex 1M solution in THF	Thermo Fisher Scientific	Cat#AC175081000; CAS 14044-65-6
Borane-d3 1M in tetrahydrofuran	Thermo Fisher Scientific	Cat#AA89121AD; CAS 13763-62-7
Ethyl 3-Phenylglycidate	TCI America	Cat#E079825G; CAS 121-39-1
(2S)-(+)-Glycidyl p-Toluenesulfonate	Thermo Fisher Scientific	Cat#AAH5600003; CAS 70987-78-9
(R)-(−)-Glycidyl butyrate	Thermo Fisher Scientific	Cat#AAL1855703; CAS 60456-26-0
N-(2,3-Epoxypropyl)phthalimide	Thermo Fisher Scientific	Cat#AC170040100; CAS 5455-98-1
Glycidyl methacrylate	Thermo Fisher Scientific	Cat#AAL1113318; CAS 106-91-2
Trimethylene Oxide	TCI America	Cat#T047310ML; CAS 503-30-0
DL-2-(4-fluorophenyl)-2-phenyltetrahydrofuran	Sigma-Aldrich	Cat #S535818; CAS 84255-03-8
Pinacolborane	Thermo Fisher Scientific	Cat#AAL1755814; CAS 25015-63-8
Lithium aluminium hydride	Thermo Fisher Scientific	Cat#AC190320100; CAS 16853-85-3
Sodium borohydride	Thermo Fisher Scientific	Cat#AA1343257; CAS 16940-66-2
Potassium borohydride	Thermo Fisher Scientific	Cat#AA3257009; CAS 13762-51-1
Lithium triethylborohydride, 1M in THF	Sigma-Aldrich	Cat#50-180-6691; CAS 22560-16-3
Sodium triethylborohydride, 1M in THF	Thermo Fisher Scientific	Cat#AC200031000; CAS 17979-81-6
Potassium triethylborohydride, 1M in THF	Thermo Fisher Scientific	Cat#AC200041000; CAS 22560-21-0
Shvo's catalyst	TCI America	Cat#H1322100MG; CAS 104439-77-2
Chloro(1,5-cyclooctadiene)rhodium(I) dimer	Thermo Fisher Scientific	Cat#AA10466MD; CAS 12092-47-6
Chloro(1,5-cyclooctadiene)iridium(I) dimer	Thermo Fisher Scientific	Cat#AA1274901; CAS 12112-67-3
Dichloro[rel-[N(S)]-N-[2-[(R)-phenylthio-κS]ethyl]-4-morpholineethananime-κNN4, κN4](triphenylphosphine)ruthenium(II)	Strem	Cat#44-0550; CAS 1799787-13-5
Carbonylchlorohydrido[6-(di-t-butylphosphinomethyl)-2-(N,N-diethylaminomethyl)pyridine]ruthenium(II)	Strem	Cat#44-0091; CAS 863971-63-5
Ru-MACHO(regR)	TCI America	Cat#R0136200MG; CAS 1295649-40-9

(*Continued on next page*)

Continued

REAGENT or RESOURCE	SOURCE	IDENTIFIER
Ru-MACHO(regR)-BH	TCI America	Cat#R0137200MG; CAS 1295649-41-0
(*S*)-(−)-Styrene oxide, 98% ee	Sigma-Aldrich	Cat#540102-5G; CAS 20780-54-5
(*R*)-(−)-α-Methoxy-α-(trifluoromethyl) phenylacetyl chloride	TCI America	Cat#M11041G; CAS 39637-99-5
Deposited data		
Structures of compounds 1-3, 5-7, 11	This paper, Cambridge Crystallographic Data Center	Databse: CCDC Nos. 2159079-2159084, 2192622
Software and algorithms		
ChemDraw Professional 16.0	PerkinElmer	https://www.perkinelmer.com/category/chemdraw
Gaussian16	Frisch et al., 2016	https://gaussian.com
Other		
Shimadzu GCMS-QP2010S	Shimadzu	https://www.ssi.shimadzu.com/products/gas-chromatograph-mass-spectrometry/single-quadrupole-gc-ms/gcms-qp2010-se/index.html
Bruker X8 Kappa Apex II diffractometer	Bruker	https://www.bruker.com/en/products-and-solutions/diffractometers-and-scattering-systems/single-crystal-x-ray-diffractometers.html
Bruker D8 VENTURE diffractometer	Bruker	https://www.bruker.com/en/products-and-solutions/diffractometers-and-scattering-systems/single-crystal-x-ray-diffractometers.html

RESOURCE AVAILABILITY

Lead contact

Further information and requests for resources should be directed to and will be fulfilled by the lead contact, Guoqi Zhang (guzhang@jjay.cuny.edu).

Materials availability

All materials generated in this study are available within the article and the Supplemental Information or from the lead contact upon reasonable request.

Data and code availability

- All data reported in this article will be available from the lead contact upon request.
- This paper does not report original code.
- Any additional information required to reanalyse the data reported in this study is available from the lead contact upon request.

METHOD DETAILS

General information

Unless specified otherwise, all reactions were carried out under a dry nitrogen atmosphere using standard glovebox. Deuterated solvents were purchased from Cambridge Isotope Laboratories. Anhydrous grade solvents (stored over 4 Å molecular sieves), alkali metal reagents and dibutylmagnesium (**C-1**), epoxide substrates and organic ligands listed in Schemes S1, S2, S3 and Figure 3 (unless otherwise stated) were all purchased from Sigma-Aldrich, Strem, Fisher Scientific and TCI America. Pinacolborane was purchased from Acros or Alfa Aesar and redistilled under reduced pressure prior to use. Ligands L5 (Vasudevan et al.,

2012), L12 (Dong et al., 2016), L13 (Dong et al., 2016), L14 (Crockett et al., 2020), L15 (Ebralidze et al., 2009), L16 (Kumar et al., 2001), and L22 (Castro et al., 2005) and complexes **C-2** (Zhang et al., 2016), **C-3** (Zhang et al., 2019a) and **C-4** (Zhang et al., 2019b) (Schemes S2 and S3) were prepared according to known procedures. Metal complexes **C5-11** (Scheme S3 and STAR Method) were purchased from Strem, Fisher Scientific and TCI America. FT-IR spectra were recorded on a Shimadzu 8400S instrument with solid samples under N_2 using a Golden Gate ATR accessory. Elemental analyses were performed by Midwest Microlab LLC in Indianapolis. ^{1}H NMR and ^{13}C NMR spectra were obtained at room temperature on a Bruker AV 500 or 600 MHz NMR spectrometer, with chemical shifts (δ) referenced to the residual solvent signal. GC-MS analysis was obtained using a Shimadzu GCMS-QP2010S gas chromatograph mass spectrometer.

Procedure for preparation of compound 1

In a glovebox under N_2, in a 20 mL scintillation vial, 2,2;6,2″-terpyridine (233 mg, 1.0 mmol) was dissolved in Et_2O (10 mL) upon rigorous stirring at room temperature. Lithium triethylborohydride (1.1 mL, 1.0 M in THF, 1.1 eq.) was added dropwise to the solution and a deep green solution developed immediately. The mixture was allowed to stir at room temperature for 4 h and then filtered. The filtrate was evaporated to ca. 3 mL and then placed in a −30°C refrigerator for 10 days. X-ray quality crystals were collected by filtration and washed with pentane (3 × 1 mL) to give green crystals. The filtrate was collected and further concentrated to ca. 2 mL and then kept at −30°C for 7 more days. Another portion of crystals was collected by filtration and washing. The combined product was dried under vacuum.

Procedure for preparation of compound 2

In a glovebox under N_2, in a 20 mL scintillation vial, 2,2;6,2″-terpyridine (233 mg, 1.0 mmol) was dissolved in Et_2O (10 mL) upon rigorous stirring at room temperature. Sodium triethylborohydride (1.1 mL, 1.0 M in THF, 1.1 eq.) was added dropwise to the solution and a dark green developed immediately. The mixture was allowed to stir at room temperature for 4 h and then filtered. The filtrate was evaporated to ca. 5 mL and then placed in a −30°C refrigerator for 3 days. X-ray quality crystals were collected by filtration and washed thoroughly with Et_2O (5 × 1 mL) and then pentane (3 × 1 mL) to give colorless crystals. The filtrate was collected and further concentrated to ca. 2 mL and then kept at −30°C for 7 more days. Another portion of crystals was collected by filtration and washing. The combined product was dried under vacuum.

Procedure for preparation of compound 3 (Figure 2)

The procedure was the same as that for synthesis of **1** except that potassium triethylborohydride (1.1 mL, 1.0 M in THF, 1.1 eq.) was used. Colorless large block-like crystals suitable for X-ray diffraction were collected and dried under vacuum.

Procedure for preparation of compound 4 (Figure 2)

In a glovebox under N_2, in a 20 mL scintillation vial, 18-crown-6 (264 mg, 1.0 mmol) was dissolved in Et_2O (10 mL) upon rigorous stirring at room temperature. Sodium triethylborohydride (1.1 mL, 1.0 M in THF, 1.1 eq.) was added dropwise to the solution and a clear colorless solution developed. The mixture was allowed to stir at room temperature for 2 h and then filtered. The filtrate was evaporated to ca. 5 mL and then placed in a −30°C refrigerator for 3 days. Colorless crystals were collected by filtration and washed with Et_2O (3 × 1 mL) and then pentane (3 × 1 mL). The product was dried under vacuum.

Procedure for preparation of compound 5 (Figure 2)

n a glovebox under N_2, in a 20 mL scintillation vial, 18-crown-6 (264 mg, 1.0 mmol) was dissolved in Et_2O (10 mL) at room temperature. Potassium triethylborohydride (1.1 mL, 1.0 M in THF, 1.1 eq.) was carefully added dropwise to the solution without stirring. Upon addition of $KHBEt_3$, fine colorless crystals appeared at the wall and the bottom. The solution was then allowed to stand at room temperature overnight, the crystals were filtered and washed with with Et_2O (3 × 1 mL) and then pentane (3 × 1 mL). The filtrate was collected and placed in a −30°C refrigerator for 7 days. X-ray quality, colorless block-like crystals were collected. The combined product was dried under vacuum.

Procedure for preparation of compound 6 (Figure 2)

In a glovebox under N_2, to a 3.8 mL vial, **2** (35.5 mg, 0.05 mmol) was added, followed by styrene oxide (30 mg, 0.25 mmol, 5 equiv.). The solid was dissolved in a minute, then toluene (1 mL) was added. The solution was mixed until a clear colorless (or greenish) solution developed. Pentane (ca. 2 mL) was carefully

layered upon the solution and then sealed. The vial was allowed to stay at −30°C for 5 days. Colorless crystals suitable for X-ray diffraction were collected and washed with pentane (3 × 1 mL). The product was dried under vacuum.

Procedure for preparation of compound 7 (Figure 2)

In a glovebox under N_2, to a 3.8 mL vial, **5** (40.2 mg, 0.1 mmol) was added, followed by styrene oxide (30 mg, 0.25 mmol, 5 equiv.). The solid was dissolved in a minute, then toluene (1 mL) was added. The solution was mixed until a clear colorless solution developed. Pentane (ca. 2 mL) was carefully layered upon the solution and then sealed. The vial was allowed to stay at −30°C for 5 days. Colorless crystals suitable for X-ray diffraction were collected and washed with pentane (3 × 1 mL). The product was dried under vacuum.

X-ray crystallography

X-ray diffraction data were collected on a Bruker X8 Kappa Apex II diffractometer using Mo Kα radiation (**1–3**, **6**), a Bruker D8 VENTURE diffractometer using Mo Kα radiation (**5**), or a Bruker D8 VENTURE diffractometer using Cu Kα radiation (**7** and **11**). Crystal data, data collection and refinement parameters are summarized in Table S1. The structures were solved using direct methods and standard difference map techniques, and were refined by full-matrix least-squares procedures on F^2 with SHELXTL (Sheldrick, 1981, 2015). All hydrogen atoms bound to carbon were placed in calculated positions and refined with a riding model [U_{iso}(H) = 1.2–1.5U_{eq}(C)], while hydrogen atoms bound to boron were located on the difference map and freely refined. For **3**, some carbon-bound hydrogen atoms involved in sigma interactions with potassium were also located on the difference map and freely refined. Database: CCDC Nos. 2159079-2159084 (**1**-**3** and **5**-**7**) and 2192622 (**11**) contain the supplementary crystallographic data for this paper. These data can be obtained free of charge via http://www.ccdc.cam.ac.uk/conts/retrieving.html, or from the Cambridge Crystallographic Data Centre, 12 Union Road, Cambridge CB2 1EZ, UK; fax: (+44) 1223-336-033; or e-mail: deposit@ccdc.cam.ac.uk.

General procedure for catalytic hydroboration of styrene oxide with various metal complexes

In a glovebox under N_2 atmosphere, catalyst **2** (0.71 mg, 0.1 mol %) and epoxide (1 mmol) was added to 1.8 mL glass vial equipped with a stir bar. Pinacolborane (141 mg, 1.1 mmol, 1.1 eq.) was then added and the reaction mixture was allowed to stir at room temperature for 2 h. After completion of the reaction, the reaction mixture was first analyzed by GC-MS to determine the regioselectivity of desired boronate esters. The results showing the comparison of the catalytic efficiency of 1–7 with various homogeneous catalysts from our laboratories (Zhang et al., 2016, 2019a), popular commercially available metal−ligand bifunctional catalysts (Dub et al., 2015; Blum et al., 1985; Kuriyama et al., 2012; Zhang et al., 2006), classical precious metal catalyst precursors, as well as $MgBu_2$ (Magre et al., 2020, 2022) being the state-of-the-art catalyst for Markovnikov epoxide hydroboration are illustrated in Scheme S3.

General procedure for 2-catalyzed hydroboration of epoxides

In a glovebox under N_2 atmosphere, catalyst **2** (0.71 mg, 0.1 mol %) and epoxide (1 mmol) was added to 1.8 mL glass vial equipped with a stir bar. Pinacolborane (141 mg, 1.1 mmol, 1.1 eq.) was then added and the reaction mixture was allowed to stir at room temperature for 2 h. After completion of the reaction, the reaction mixture was first analyzed by GC-MS to determine the regioselectivity of desired boronate esters. The reaction mixture was quenched with aq. $NaHCO_3$, and then extracted with Et_2O. The crude reaction mixture then subject to a flash column chromatography on silica using ethyl acetate/hexane as an eluent. The pure products of alcohols were obtained and characterized by ^1H and ^{13}C NMR spectroscopies (Figure 3).

Procedure for synthesis of 2-((1-chloropropan-2-yl)oxy)-4,4,5,5-tetramethyl-1,3,2-dioxaborolane (9w, Figure 3)

In a glovebox under N_2 atmosphere, catalyst **2** (0.71 mg, 1.0 μmol) was placed in a 1.5 mL glass vial equipped with a stir bar. 2-((Allyloxy)methyl)oxirane (92.5 mg, 1.0 mmol) and pinacolborane (141 mg, 1.1 mmol, 1.1 eq.) were then added. Hexamethylbenzene (3.0 mg) was added as an internal standard. The reaction mixture was allowed to stir at room temperature for 2 h and then transferred to an NMR tube containing $CDCl_3$ for measurement.

Procedure for synthesis of 2,2′-(propane-1,2-diylbis(oxy))bis(4,4,5,5-tetramethyl-1,3,2-dioxaborolane) (9x, Figure 3)

In a glovebox under N_2 atmosphere, catalyst **2** (0.71 mg, 1.0 μmol) was placed in a 1.5 mL glass vial equipped with a stir bar. Glycidol (0.74 mg, 1.0 mmol) and pinacolborane (282 mg, 2.2 mmol, 2.2 eq.) were then added. Hexamethylbenzene (2.8 mg) was added as an internal standard. The reaction mixture was allowed to stir at room temperature for 2 h and then transferred to an NMR tube containing $CDCl_3$ for measurement.

Procedure for synthesis of 1,2-diphenylethan-1-ol (9y, Figure 3)

In a glovebox under N_2 atmosphere, catalyst **2** (0.71 mg, 1.0 μmol) was placed in a Schlenk tube equipped with a stir bar. Trans-stilbene oxide (196 mg, 1.0 mmol) and pinacolborane (141 mg, 1.1 mmol, 1.1 eq.) and THF (2 mL) were then added. The reaction mixture was allowed to stir at 80°C for 16 h. The reaction was exposed to the air and quenched with aq. $NaHCO_3$, and then extracted with Et_2O. The organic phase was purified through a column chromatography (silica gel) using ethyl acetate/hexane (1:20, v/v) as an eluent.

Procedure for synthesis of 4,4,5,5-tetramethyl-2-propoxy-1,3,2-dioxaborolane (10, Figure 3)

In a glovebox under N_2 atmosphere, catalyst **2** (0.71 mg, 1.0 μmol) was placed in a 1.5 mL glass vial equipped with a stir bar. Trimethylene oxide (58.0 mg, 1.0 mmol) and pinacolborane (141 mg, 1.1 mmol, 1.1 eq.) were then added. Hexamethylbenzene (6 mg) was added as an internal standard. The reaction mixture was allowed to stir at room temperature for 1 h and then transferred to an NMR tube containing $CDCl_3$ for measurement.

Gram-scale experiment for 2-catalyzed hydroboration of 2-(phenoxymethyl)oxirane

In a glovebox under N_2 atmosphere, catalyst **2** (5.4 mg, 0.1 mol%) was placed in a 20 mL glass vial equipped with a tiny stir bar. 2-(Phenoxymethyl)oxirane (1.5 g, 10 mmol) and pinacolborane (1.41 g, 11 mmol, 1.1 eq) were then added. The reaction mixture was allowed to stir at room temperature for 2 h. The reaction was exposed to the air and quenched with aq. $NaHCO_3$, and then extracted with Et_2O. The crude reaction mixture was analyzed by GC-MS (92% GC yield) and then the product was isolated (1.34 g, 88%) by column chromatography (silica gel) using ethyl acetate/hexane (1:10, v/v) as an eluent. The product was characterized by ^1H and ^{13}C NMR spectroscopies (Scheme S4).

4,4,5,5-Tetramethyl-2-(phenyl(3-phenyloxiran-2-yl)methoxy)-1,3,2-dioxaborolane (11)

In a glovebox under N_2 atmosphere, catalyst **2** (0.71 mg, 1.0 μmol) was placed in a 3.8 mL glass vial equipped with a stir bar. 1,3-Diphenyl-2,3-epoxy-1-propanone (224 mg, 1.0 mmol), pinacolborane (141 mg, 1.1 mmol, 1.1 eq.) and THF (1.5 mL) were then added were then added. The reaction mixture was allowed to stir at room temperature for 16 h to give white suspension. The solid was filtered and washed with Et_2O and then dried under vaccuum. White solid was isolated. Yield: 89 mg (92%). X-ray quality crystals were obtained by slow evaporation of a dichloromethane/THF solution (Figure S7).

Procedure for preparation of Mosher ester, (R)-1-phenylethyl (R)-3,3,3-trifluoro-2-methoxy-2-phenylpropanoate

In a glovebox under N_2 atmosphere, catalyst **2** (0.71 mg, 1.0 μmol) was placed in a 1.5 mL glass vial equipped with a stir bar. (*S*)-(−)-Styrene oxide (120 mg, 1.0 mmol, 98% ee) and pinacolborane (141 mg, 1.1 mmol, 1.1 eq.) were then added. The reaction mixture was allowed to stir at room temperature for 2 h. The reaction was exposed to the air and quenched with aq. $NaHCO_3$, and then extracted with Et_2O. The organic phase was purified through a column chromatography (silica gel) using ethyl acetate/hexane (1:20, v/v) as an eluent. Colorless oil was isolated (92%). The product was subject to the reaction with (*R*)-(−)-α-Methoxy-α-(trifluoromethyl)phenylacetyl chloride to give the desired Mosher ester for determination of enatiomeric excess by ^1H NMR (in comparison with the ^1H NMR of the diastereomeric mixture made from racemic 1-phenylethanol and (*R*)-(−)-α-Methoxy-α-(trifluoromethyl)phenylacetyl chloride) (Scheme S7).

Deuterium-labeling experiment

1-Phenylethan-2-*d*-1-ol (**[D]-9a**): In a glovebox under N_2 atmosphere, BD_3·THF (2 mL, 1 M in THF) was diluted with 1 mL THF. The solution was then added dropwise over 15 min to a 0°C solution of pinacol (236 mg, 2 mmol) in 1 mL THF. After the completion of addition, the solution was warmed up to room temperature and then stirred for additional 2 h. To this solution, catalyst **2** (1.42 mg, 0.1 mol %) and

styrene oxide (240 mg, 2 mmol) were then added and the solution was stirred for 1 h at room temperature. After GC analysis was conducted, the reaction was quenched with aq. $NaHCO_3$, and then extracted with Et_2O. The crude product was purified through a column chromatography (silica gel) using ethyl acetate/hexane (1:20, v/v) as an eluent. Colorless oil of **[D]-9a** was isolated. Yield: 221 mg (90%). ^{1}H NMR (400 MHz, Chloroform-*d*) δ ^{1}H NMR (400 MHz, $CDCl_3$) δ 7.37 – 7.30 (m, 4H), 7.28 – 7.23 (m, 1H), 4.84 (t, J = 6.1 Hz, 1H), 2.20 (br, 1H), 1.48-1.43 (m, 2H) ppm; ^{13}C NMR (151 MHz, $CDCl_3$) δ 146.0, 128.6, 127.5, 125.5, 70.4, 25.0 (t, $^1J_{C\text{-}D}$ = 19.5 Hz) ppm. GC-MS (m/z): 123 (calc. 123). Note: In a separate control experiment, the reaction was carried out using the in-situ formed DBpin without the addition of catalyst **2**. Thus, styrene oxide (240 mg, 2 mmol) was directly added to the solution of DBpin formed in-situ and the mixture was stirred for 1 h at room temperature. Then, GC-MS analysis was conducted with hexamethylbenzene as an internal standard (Scheme S9).

Kinetics experiments

Initial rates versus concentration of styrene oxide 8a in THF. In a glovebox under N_2 atmosphere, a stock solution containing catalyst **2** (5.9 mg) and HBpin (460 mg) in THF (the total volume = 3.2 mL) was prepared. The solution was equally divided into 8 small vials equipped with stir bars. Various concentrations of styrene oxide as indicated were then added to each vial and then hexamethylbenzene (2.09 mg) as internal standard for GC analysis was added. The reaction mixture was allowed to stir at 25°C. Aliquots for the GC analysis were withdrawn from each reaction mixture upon quenching of reactions by methanol after 5 minutes. The data are summarized in Table S3. The rate constant k was calculated as an average of k obtained in three experiments.

Initial rates versus concentration of HBpin in THF. In a glovebox under N_2 atmosphere, a stock solution containing catalyst **2** (12.5 mg) and styrene oxide (557 mg) in THF (the total volume = 5 mL) was prepared. The solution was equally divided into 10 small vials equipped with stir bars. Various concentrations of HBpin as indicated were then added to each vial and then hexamethylbenzene (0.95 mg) as internal standard for GC analysis was added. The reaction mixture was allowed to stir at 25°C. Aliquots for the GC-MS analysis were withdrawn from each reaction mixture after 5 minutes. The data are summarized in Table S4.

Initial rates versus concentration of 2 in THF. In a glovebox under N_2 atmosphere, a stock solution containing styrene oxide (755 mg) and HBpin (556 mg) in THF (the total volume = 3.7 mL) was prepared. The solution was equally divided into 8 small vials equipped with stir bars. Various concentrations of **2** as indicated were then added to each vial and then hexamethylbenzene (2.8 mg) as internal standard for GC analysis was added. The reaction mixture was allowed to stir at 25°C. Aliquots for the GC analysis were withdrawn from each reaction mixture after 5 minutes. The data are summarized in Table S5.

Rate law expression. Taking into account known accuracy limitations of initial rates method, the reaction can be approximately described by the following rate equation: d[product]/dt $\sim$ k[styrene oxide]^1[HBpin]^1[**2**]$^{0.5}$ with $k \approx 0.39$ min^{-1} M$^{-1.5}$ at 25°C. The rate consant k was calculated as an average of k obtained in three experiments.

Computational analysis

All calculations were performed with Gaussian 16 (rev. C01) software (Frisch et al., 2016). Hybrid ωB97X-D (Chai and Head-Gordon, 2008) (with 100 and 22% exchange at long and short ranges, respectively) functional implementing built-in D2 correction term (Grimme, 2006) was employed. To introduce non-specific solvent effects of THF in the geometry optimization steps, the Solvation Model based on Density (SMD) (Marenich et al., 2009), a popular version of a polarizable continuum model, was used. All the geometries were optimized with the def2-svp and further refined with the def2-qzvp basis, respectively. The standard reaction Gibbs energies (1M, 298K) were calculated by combining the single-point def2-svp//def2-qzvp energies with the thermal corrections from frequency calculations under def2-SVP level, adjusted by 0.00301 Hartree and converted to kcal•mol^{-1}. Various transition states were sampled with constrained potential energy surface scan and further optimized by using Berny algorithm. We report only the lowest energy located transition states for each scenario and/or relevant for discussion cases. Molecular graphics images were produced using the UCSF Chimera package (Pettersen et al., 2004). Table S6 contains information on energy data.

Origin of regioselectivity for 9f. Figure S11 shows optimized transition states leading to Markovnikov and *anti*-Markovnikov products of **9f** with $[HBEt_3]^-$, $[HBEt_3]^-Na^+$ and $[HBEt_3]^-Na^+$(**L17**) catalysts alone or in the presence of 1 equiv of HBpin. For each catalyst, we considered a bimolecular catalyst–**9f** complex (e.g. transition state TS_A, TS_G, TS_M, TS_D, TS_J and TS_P), or a trimolecular catalyst–**9f**–HBpin complex (e.g. remaining transition states). In the latter case, HBpin can form a B–O bond as a result of a concerted trimolecular process (e.g. transition state TS_B, TS_E, TS_H, TS_K, TS_N and TS_Q), or serve as a shuttle to deliver a hydride (e.g. transition state TS_C, TS_F, TS_I, TS_L, TS_O and TS_R) via an $[(HBpin)HBEt_3]^-$ adduct, whose formation is endergonic but kinetically accesible (e.g. for example $\Delta G°_{298K,\ r}$ = 5.7 kcal mol^{-1} for $[(HBpin)HBEt_3]^-Na^+$ formation relative to HBpin and $[HBEt_3]^-Na^+$). The hydride transfer from HBpin via a shuttle to C-epoxide seems to be always energetically unfavorable (e.g. transition state TS_C, TS_F, TS_I, TS_L, TS_O and TS_R) over HBpin-assisted hydride transfer from $[HBEt_3]^-$ (e.g. transition state TS_B, TS_E, TS_H, TS_K, TS_N and TS_Q). Thus, bimolecular catalyst–**9f** complexes (e.g. transition state TS_A, TS_G, TS_M, TS_D, TS_J and TS_P) and/or trimolecular catalyst–**9f**–HBpin complexes (e.g. transition state TS_B, TS_E, TS_H, TS_K, TS_N and TS_Q) are energetically possible. Of those, the most favorable ones are summarized in Figure 4.

We also note here that for the $[HBEt_3]^-Na^+$ catalyst, Na^+ can be placed anywhere in the initial guess for the geometry optimization. Located transition states TS_G–TS_L represent the lowest energy pathways. Transition states that were sampled from the $[HBEt_3]^-Na^+$ contact ion pair were found to be uniformally less-stable on average by 3–4 kcal mol^{-1}, i.e. the cases when Na^+ was always in close proximity to the hydride donor, consistent with the fact that Na^+ cannot establish any non-covalent interactions with the opposite site of the molecule within transition state structures.

Origin of regioselectivity for 9a. Catalytic cycle for 8a hydroboration. Figure S12 provides additional information for optimized transition states leading to Markovnikov-product **9a** formation with the $[HBEt_3]^-Na^+$(**L17**) catalyst. Transition states TS_1, TS_3 and TS_6 are structurally similar to TS_N, TS_M and TS_O, respectively. Here we also report an additional transition state, TS_5, which is a spatial isomer of transition state TS_1 for a trimolecular catalyst–**8a**–HBpin complex. As expected, the isomer TS_1 is more energetically favorable, which is most likely the result of both cation-substrate//HBpin non-covalent ionic interaction and π-π catalyst-substrate stacking interaction. TS_3 represents a bimolecular catalyst–**8a** complex, whereas in TS_6 HBpin serves as a shuttle to deliver a hydride. Similar to **9f** (see Results and discussion above), this hydride transfer from HBpin via a shuttle to C-epoxide seems to be energetivally unfavorable. Thus, in the catalytic cycle for **8a**, only two transition states TS_1 and TS_3 are energetically accesible. Taking into account the DFT accuracy, they are indistinguishable, which offers the possibility of two catalytic cycles connected with shared intermediates (branching points). Figure S13 shows these catalytic cycles that are possible for **8a** hydroboration with **2** leading to Markovnikov-product **9a** based on the standard ~3 kcal mol^{-1} accuracy of DFT (Dub and Gordon, 2017). Two pathways **A** and **B** are connected through **int0** and **int1a** branching points. Although both pathways are indistinguishable by computations, the pathways differ by the molecularity of the rate- and regioselectivity-determining transition states and thus predicted rate law expression. Only pathway **A** is consistent with the experimental rate law rate of $\sim k$[styrene oxide]^1[HBpin]^1[**2**]$^{0.5}$ (Kozuch et al., 2009). This pathway **A** is drawn in Figure 4B and represents the proposed catalytic cycle for the reaction under study.

Spectroscopic details

Compound 1 (Figure 2). Yield: 73.5 mg (22%). FT-IR (solid, cm^{-1}): 2928s, 2890s, 2850s, 1590s, 1577s, 1469s, 1445s, 1402m, 1242m, 1153m, 1049m, 999m, 960m. ^{1}H NMR (600 MHz, THF-d_8) δ 8.68 – 8.63 (m, 4H), 8.63 – 8.57 (m, 4H), 8.50 (dd, J = 7.9, 1.9 Hz, 4H), 8.03 – 7.98 (m, 2H), 7.90 (ddd, J = 9.6, 5.8, 2.0 Hz, 4H), 7.36 (ddd, J = 7.4, 4.7, 1.3 Hz, 4H), 1.03 (dd, J = 7.4, 4.4 Hz, 4H), 0.90 (d, J = 9.3 Hz, 8H), 0.79 – 0.58 (m, 12H), 0.03 (dd, J = 7.6, 2.8 Hz, 6H) ppm. ^{13}C NMR (151 MHz, THF-d_8) δ 156.8, 156.3, 150.4, 150.2, 139.0, 137.9, 125.0, 121.8, 11.5, 11.1 ppm. Elemental analysis calc. (%) for $C_{42}H_{53}B_2LiN_6$: C 75.24, H 7.97, N 12.53; Found C 75.75, H 7.52, N 12.36.

Compound 2 (Figure 2). Yield: 231 mg (65%). FT-IR (solid, cm^{-1}): 2927s, 2890s, 2838s, 1908s, 1590m, 1578m, 1445s, 1430s, 1307w, 1241w, 1153s, 1099w, 1046w, 998m, 931w. ^{1}H NMR (500 MHz, THF) δ 8.74 – 8.60 (m, 4H), 8.52 (d, J = 7.7 Hz, 2H), 7.96 (t, J = 7.9 Hz, 1H), 7.87 (t, J = 7.8 Hz, 2H), 7.34 (dd, J = 7.8, 4.5 Hz, 2H), 0.70 (t, J = 7.9 Hz, 9H), −0.02 (q, J = 7.9 Hz, 6H) ppm. ^{13}C NMR (126 MHz, THF) δ 157.2,

156.5, 150.2, 138.6, 137.6, 124.7, 121.8, 121.6, 15.9, 11.2 ppm. Elemental analysis calc. (%) for $C_{42}H_{54}B_2Na_2N_6$: C 71.00, H 7.66, N 11.83; Found C 70.82, H 7.18, N 11.96.

Compound 3 (Figure 2). Yield: 267 mg (72%). FT-IR (solid, cm^{-1}): 2886s, 2839s, 2794s, 2027m, 1979m, 1587s, 1570s, 1475s, 1443s, 1428s, 1305w, 1239w, 1165m, 1152m, 1090s, 1051m, 997m, 936w. ^{1}H NMR (600 MHz, THF-d_8) δ 8.69 – 8.62 (m, overlapping, 8H), 8.52 (d, J = 7.7 Hz, 4H), 7.96 (t, J = 7.8 Hz, 2H), 7.87 (td, J = 7.7, 1.9 Hz, 4H), 7.33 (ddd, J = 74.5, 4.6, 1.3 Hz, 4H), 0.70 (dt, J = 44.3, 7.1 Hz, 18H), 0.07 – -0.06 (dq, J = 41.4, 7.5 Hz, 12H) ppm. ^{13}C NMR (151 MHz, THF-d_8) δ 157.2, 156.5, 150.2, 138.6, 137.6, 124.7, 121.8, 121.6, 14.2, 11.5 (d, J = 8 Hz) ppm. Elemental analysis calc. (%) for $C_{42}H_{54}B_2K_2N_6$: C 67.92, H 7.33, N 11.31; Found C 67.72, H 7.03, N 11.37.

Compound 4 (Figure 2). Yield: 347 mg (90%). FT-IR (solid, cm^{-1}): 2887s, 2837s, 2788s, 2078w, 1471m, 1454m, 1285w, 1250s, 1106s, 965s. ^{1}H NMR (500 MHz, Tol- d_8) δ 3.14 (s, 24H), 1.50 (q, J = 6.2 Hz, 9H), 0.82 – 0.73 (m, 6H) ppm. ^{13}C NMR (126 MHz, THF) δ 71.7, 15.9, 15.1 ppm. Elemental analysis calc. (%) for $C_{18}H_{40}BNaO_6$: C 55.96, H 10.44; Found C 55.65, H 10.22.

Compound 5 (Figure 2). Yield: 354 mg (88%). FT-IR (solid, cm^{-1}): 2886s, 2835s, 2787m, 2074w, 1979m, 1470m, 1455m, 1351s, 1285m, 1250m, 1103s, 961s. ^{1}H NMR (500 MHz, Tol-d_8) δ 3.14 (s, 24H), 1.55 – 1.43 (m, 9H), 0.82 – 0.73 (m, 6H) ppm. ^{13}C NMR (126 MHz, Tol-d_8) δ 70.5, 15.9, 15.1 ppm. Elemental analysis calc. (%) for $C_{18}H_{40}BKO_6$: C 53.72, H 10.02; Found C 53.37, H 9.88.

Compound 6 (Figure 2). Yield: 267 mg (86%). FT-IR (solid, cm^{-1}): 2923m, 2890m, 2849s, 2793s, 1589s, 1579s, 1473s, 1444s, 1430s, 1400w, 1304w, 1240m, 1185w, 1155s, 1119m, 1262m, 998s, 947m. ^{1}H NMR (600 MHz, THF) δ 8.66 (dd, J = 7.2, 1.6 Hz, 4H), 8.52 (d, J = 8.0 Hz, 2H), 7.96 (t, J = 7.8 Hz, 1H), 7.88 – 7.84 (m, 2H), 7.37 – 7.29 (m, 4H), 7.24 (t, J = 7.6 Hz, 2H), 7.17 – 7.10 (m, 1H), 4.73 (t, J = 6.4 Hz, 1H), 1.35 (d, J = 6.4 Hz, 3H), 0.69 (p, J = 7.3 Hz, 9H), −0.05 (q, J = 7.7 Hz, 6H) ppm. ^{13}C NMR (151 MHz, THF) δ 157.2, 156.5, 150.2, 138.6, 137.6, 128.9, 127.4, 126.2, 124.7, 121.8, 121.6, 11.2 ppm. Elemental analysis calc. (%) for $C_{29}H_{35}BN_3NaO$: C 73.27, H 7.42, N 8.84; Found C 73.65, H 7.56, N 8.38.

Compound 7 (Figure 2). Yield: 44.4 mg (85%). FT-IR (solid, cm^{-1}): 2886s, 2835s, 2787m, 2074w, 1979m, 1470m, 1455m, 1351s, 1285m, 1250m, 1103s, 961s. ^{1}H NMR (500 MHz, Tol-d_8) δ 7.77 – 7.69 (m, 2H), 7.30 – 7.22 (m, 2H), 7.15 – 7.11 (m, 1H), 5.26 (q, J = 6.5 Hz, 1H), 3.11 (s, 25H), 1.56 (d, J = 6.4 Hz, 3H), 1.34 (t, J = 7.7 Hz, 9H), 0.69 (dd, J = 7.7, 5.7 Hz, 6H) ppm. ^{13}C NMR (126 MHz, THF) δ 154.1, 127.0, 126.7, 69.3, 68.0, 28.3, 15.2, 12.0 ppm. Elemental analysis calc. (%) for $C_{26}H_{48}BKO_7$: C 59.76, H 9.26; Found C 59.32, H 9.12.

1-Phenylethanol (9a, Figure 3) (Thiyagarajan and Gunanathan, 2019). The general procedure was followed. Colorless oil was isolated. Yield: 116 mg (95%). ^{1}H NMR (400 MHz, Chloroform-d) δ ^{1}H NMR (400 MHz, $CDCl_3$) δ 7.27 – 7.09 (m, 5H), 4.72 (q, J = 6.5 Hz, 1H), 2.10 (s, 1H), 1.34 (d, J = 6.5 Hz, 3H) ppm; ^{13}C NMR (101 MHz, $CDCl_3$) δ 145.9, 128.6, 127.5, 125.5, 70.4, 25.2 ppm.

1-(4-Fluorophenyl)ethanol (9b, Figure 3) (Thiyagarajan and Gunanathan, 2019). The general procedure was followed. Colorless oil was isolated. Yield: 119 mg (85%). ^{1}H NMR (400 MHz, $CDCl_3$) δ 7.31 (dd, J = 8.5, 5.5 Hz, 2H), 7.01 (t, J = 8.7 Hz, 2H), 4.85 (q, J = 6.5 Hz, 1H), 2.17 (s, 1H), 1.45 (d, J = 6.5 Hz, 3H) ppm; ^{13}C NMR (101 MHz, $CDCl_3$) δ 163.4, 161.0, 141.7, 141.6, 127.2, 127.1, 115.5, 115.2, 69.8, 25.4 ppm.

1-(4-Chlorophenyl)ethanol (9c, Figure 3) (Thiyagarajan and Gunanathan, 2019). The general procedure was followed. White solid was isolated. Yield: 146 mg (93%). ^{1}H NMR (400 MHz, $CDCl_3$) δ 7.26 (q, J = 8.5 Hz, 4H), 4.79 (q, J = 6.5 Hz, 1H), 2.63 (s, 1H), 1.41 (d, J = 6.5 Hz, 3H) ppm; ^{13}C NMR (101 MHz, $CDCl_3$) δ 144.3, 133.1, 128.6, 126.9, 69.7, 25.3 ppm.

2-Octanol (9d, Figure 3) (Thiyagarajan and Gunanathan, 2019). The general procedure was followed. Colorless oil was isolated. Yield: 109 mg (84%). ^{1}H NMR (400 MHz, $CDCl_3$) δ 3.87 – 3.71 (m, 1H), 1.74 (s, 1H), 1.51 – 1.25 (m, 10H), 1.18 (d, J = 6.2 Hz, 3H), 0.93 – 0.83 (m, 3H) ppm; ^{13}C NMR (101 MHz, $CDCl_3$) δ 68.2, 39.5, 31.9, 29.4, 25.9, 23.5, 22.7, 14.2 ppm.

2-Dodecanol (9e, Figure 3) (Thiyagarajan and Gunanathan, 2019). The general procedure was followed. Colorless oil was isolated. Yield: 160 mg (86%). ^{1}H NMR (600 MHz, $CDCl_3$) δ 3.83 – 3.72 (m, 1H), 1.77 (s, 1H), 1.49 – 1.23 (m, 18H), 1.18 (d, J = 6.3 Hz, 3H), 0.88 (t, J = 7.0 Hz, 3H) ppm; ^{13}C NMR (151 MHz, $CDCl_3$) δ 68.2, 39.5, 32.0, 29.8, 29.8, 29.7, 29.5, 25.9, 23.5, 22.8, 14.2 ppm.

1-Phenoxypropan-2-ol (9f, Figure 3) (Thiyagarajan and Gunanathan, 2019). The general procedure was followed. Colorless oil was isolated. Yield: 143 mg (94%). ^{1}H NMR (600 MHz, $CDCl_3$) δ 7.28 (dd, J = 8.7, 7.3 Hz, 2H), 6.96 (d, J = 1.2 Hz, 1H), 6.93 – 6.86 (m, 2H), 4.25 – 4.12 (m, 1H), 3.93 (dd, J = 9.2, 3.2 Hz, 1H), 3.79 (dd, J = 9.3, 7.6 Hz, 1H), 2.45 (s, 1H), 1.27 (d, J = 6.5 Hz, 3H) ppm; ^{13}C NMR (151 MHz, $CDCl_3$) δ 158.7, 129.7, 121.3, 114.7, 73.4, 66.4, 18.9 ppm.

1-(2-Methylphenoxy)propan-2-ol (9g, Figure 3) (Thiyagarajan and Gunanathan, 2019). The general procedure was followed. White solid was isolated. Yield: 147 mg (92%). ^{1}H NMR (600 MHz, $CDCl_3$) δ 7.21 – 7.08 (m, 2H), 6.87 (td, J = 7.4, 1.1 Hz, 1H), 6.83 – 6.74 (m, 1H), 4.20 (dt, J = 6.7, 3.4 Hz, 1H), 3.92 (dd, J = 9.2, 3.5 Hz, 1H), 3.80 (dd, J = 9.3, 7.3 Hz, 1H), 2.42 (s, 1H), 2.24 (s, 3H), 1.29 (d, J = 6.5 Hz, 3H) ppm; ^{13}C NMR (151 MHz, $CDCl_3$) δ 156.7, 130.9, 127.0, 126.9, 121.0, 111.4, 73.5, 66.6, 19.0, 16.3 ppm.

1-(2-Methoxyphenoxy)propan-2-ol (9h, Figure 3) (Thiyagarajan and Gunanathan, 2019). The general procedure was followed. Yellowish solid was isolated. Yield: 171 mg (94%). ^{1}H NMR (600 MHz, $CDCl_3$) δ 6.99 – 6.92 (m, 2H), 6.90 (ddd, J = 8.0, 3.9, 2.3 Hz, 2H), 4.22 – 4.13 (m, 1H), 4.00 (dd, J = 9.7, 3.0 Hz, 1H), 3.85 (s, 3H), 3.79 (dd, J = 9.7, 8.3 Hz, 1H), 3.09 (s, 1H), 1.24 (d, J = 6.3 Hz, 3H) ppm; ^{13}C NMR (151 MHz, $CDCl_3$) δ 150.2, 148.4, 122.4, 121.2, 115.8, 112.2, 66.1, 56.0, 18.5 ppm.

1-(4-Methoxyphenoxy)propan-2-ol (9i, Figure 3) (Thiyagarajan and Gunanathan, 2019). The general procedure was followed. Yellowish solid was isolated. Yield: 173 mg (95%). ^{1}H NMR (600 MHz, $CDCl_3$) δ 6.83 (d, J = 9.1 Hz, 2H), 6.81 (d, J = 9.5 Hz, 2H), 4.14 (tq, J = 6.6, 3.3 Hz, 1H), 3.86 (dd, J = 9.2, 3.4 Hz, 1H), 3.75 (s, 3H), 3.73 (d, J = 9.3 Hz, 1H), 2.67 (s, 1H), 1.24 (s, 3H) ppm; ^{13}C NMR (151 MHz, $CDCl_3$) δ 154.2, 152.9, 115.7, 114.8, 74.2, 66.3, 55.8, 18.9 ppm.

1-(2,4-Dibromophenoxy)propan-2-ol (9j, Figure 3) (Thiyagarajan and Gunanathan, 2019). The general procedure was followed. Yellowish solid was isolated. Yield: 285 mg (92%). ^{1}H NMR (600 MHz, $CDCl_3$) δ 7.66 (d, J = 2.4 Hz, 1H), 7.36 (dd, J = 8.7, 2.4 Hz, 1H), 6.76 (d, J = 8.7 Hz, 1H), 4.23 (dt, J = 6.9, 3.5 Hz, 1H), 3.98 (dd, J = 9.1, 3.3 Hz, 1H), 3.81 (dd, J = 9.1, 7.4 Hz, 1H), 2.49 (d, J = 3.5 Hz, 1H), 1.30 (d, J = 6.5 Hz, 3H) ppm; ^{13}C NMR (151 MHz, $CDCl_3$) δ 154.4, 135.7, 131.5, 115.0, 113.7, 113.5, 66.2, 18.8 ppm.

1-(Benzyloxy)propan-2-ol (9k, Figure 3) (Thiyagarajan and Gunanathan, 2019). The general procedure was followed. Colorless oil was isolated. Yield: 150 mg (90%). ^{1}H NMR (400 MHz, $CDCl_3$) δ 7.42 – 7.21 (m, 5H), 4.53 (s, 2H), 4.07 – 3.87 (m, 1H), 3.43 (dd, J = 9.4, 3.2 Hz, 1H), 3.27 (dd, J = 9.4, 8.0 Hz, 1H), 2.72 (s, 1H), 1.13 (d, J = 6.4 Hz, 3H) ppm; ^{13}C NMR (101 MHz, $CDCl_3$) δ 138.0, 128.5, 127.8, 127.8, 75.9, 73.3, 66.5, 18.8 ppm.

1-([1,1′-Biphenyl]-2-yloxy)propan-2-ol (9l, Figure 3) (Thiyagarajan and Gunanathan, 2019). The general procedure was followed. White solid was isolated. Yield: 210 mg (92%). ^{1}H NMR (400 MHz, $CDCl_3$) δ 7.54 – 7.46 (m, 2H), 7.39 (td, J = 7.1, 6.2, 1.2 Hz, 2H), 7.35 – 7.26 (m, 3H), 7.05 (td, J = 7.5, 1.1 Hz, 1H), 6.96 (dd, J = 8.2, 1.1 Hz, 1H), 4.09 – 3.97 (m, 1H), 3.93 (dd, J = 9.2, 3.3 Hz, 1H), 3.73 (dd, J = 9.2, 7.6 Hz, 1H), 2.17 (s, 1H), 1.16 (d, J = 6.5 Hz, 3H) ppm; ^{13}C NMR (101 MHz, $CDCl_3$) δ 155.5, 138.5, 131.5, 131.0, 129.5, 128.8, 128.2, 127.2, 121.7, 113.4, 74.3, 66.3, 18.7 ppm.

1-(4-Chlorophenyl)-3,4,4-trimethylpentan-3-ol (9m, Figure 3). The general procedure was followed. Colorless oil was isolated. Yield: 197 mg (82%). ^{1}H NMR (600 MHz, $CDCl_3$) δ 7.17 (d, J = 8.4 Hz, 2H), 7.07 (d, J = 8.4 Hz, 2H), 2.69 (ddd, J = 13.5, 12.1, 4.7 Hz, 1H), 2.56 (ddd, J = 13.5, 12.2, 5.4 Hz, 1H), 1.73 (dddd, J = 13.9, 12.2, 4.7, 0.8 Hz, 1H), 1.63 (ddd, J = 13.8, 12.2, 5.4 Hz, 1H), 1.14 (d, J = 0.9 Hz, 3H), 0.88 (s, 9H) ppm; ^{13}C NMR (151 MHz, $CDCl_3$) δ 141.8, 131.5, 129.9, 128.6, 38.5 38.3, 30.1, 25.4, 21.1, 21.1 ppm. Anal. Calc. for $C_{14}H_{21}ClO$, C 69.84, H 8.79%; Found C 70.22, H 8.96%.

*1-(3-(Triethoxysilyl)propoxy)propan-2-ol (**9n**, Figure 3).* The general procedure was followed. Colorless oil was isolated. Yield: 257 mg (92%). ^{1}H NMR (600 MHz, $CDCl_3$) δ 3.90 (ddt, J = 8.1, 4.9, 1.7 Hz, 1H), 3.78 (q, J = 7.0 Hz, 6H), 3.45 – 3.34 (m, 3H), 3.17 (dd, J = 9.5, 8.1 Hz, 1H), 2.45 (br., 1H), 1.66 (ddt, J = 9.9, 8.3, 6.6 Hz, 2H), 1.18 (t, J = 7.0 Hz, 9H), 1.09 (d, J = 6.4 Hz, 3H), 0.65 – 0.58 (m, 2H) ppm; ^{13}C NMR (126 MHz, $CDCl_3$) δ 76.4, 73.5, 66.4, 58.5, 24.9, 24.7, 23.1, 18.7, 18.4, 6.7 ppm. Elemental analysis calc. (%) for $C_{12}H_{28}O_5Si$: C 51.40, H 10.06; Found C 51.75, H 10.17.

Cyclohexanol (9o, Figure 3) (Magre et al., 2020). The general procedure was followed. Colorless oil was isolated. Yield: 80 mg (80%). ^{1}H NMR (500 MHz, $CDCl_3$) δ 3.60 (dt, J = 9.3, 4.9 Hz, 1H), 2.02 – 1.95 (m, 1H), 1.94 – 1.84 (m, 2H), 1.79 – 1.68 (m, 2H), 1.60 – 1.50 (m, 1H), 1.31 – 1.21 (m, 4H), 1.18 (ddd, J = 11.8, 8.6, 5.2 Hz, 1H) ppm; ^{13}C NMR (151 MHz, $CDCl_3$) δ 70.4, 35.6, 25.6, 24.3 ppm.

1-(2,2,3,3-Tetrafluoropropoxy)propan-2-ol (9p, Figure 3). The general procedure was followed. Colorless oil was isolated. Yield: 161 mg (85%). ^{1}H NMR (600 MHz, $CDCl_3$) δ 5.92 (tt, J = 53.2, 4.7 Hz, 1H), 4.04 – 3.94 (m, 1H), 3.89 (tt, J = 12.7, 1.7 Hz, 2H), 3.57 (dd, J = 9.6, 3.2 Hz, 1H), 3.41 (dd, J = 9.6, 7.6 Hz, 1H), 2.22 (s, 1H), 1.16 (d, J = 6.4 Hz, 3H) ppm; ^{13}C NMR (151 MHz, $CDCl_3$) δ 111.1 (t, J = 35.3 HZ), 109.4 (t, J = 35.3 HZ), 78.3, 68.4 (t, J = 28.1 HZ), 66.6 (d, J = 5.8 Hz), 18.7 ppm. Elemental analysis calc. (%) for $C_6H_{10}F_4O_2$: C 37.90, H 5.30; Found C 38.25, H 5.58.

1-(Furan-2-methoxy)propan-2-ol (9q, Figure 3) (Molander and McKie, 1992). The general procedure was followed. Colorless oil was isolated. Yield: 142 mg (91%). ^{1}H NMR (600 MHz, $CDCl_3$) δ 7.40 (d, J = 1.9 Hz, 1H), 6.38 – 6.27 (m, 2H), 4.52 – 4.44 (m, 2H), 3.94 (ddd, J = 8.1, 6.4, 3.1 Hz, 1H), 3.45 (dd, J = 9.5, 3.2 Hz, 1H), 3.27 (dd, J = 9.6, 8.0 Hz, 1H), 2.54 (s, 1H), 1.12 (d, J = 6.6 Hz, 3H) ppm; ^{13}C NMR (151 MHz, $CDCl_3$) δ 151.7, 142.9, 110.4, 109.5, 75.7, 66.4, 65.1, 18.7 ppm.

Dec-9-en-2-ol (9r, Figure 3) (Thiyagarajan and Gunanathan, 2019). The general procedure was followed. Colorless oil was isolated. Yield: 136 mg (87%). ^{1}H NMR (600 MHz, $CDCl_3$) δ 5.80 (ddt, J = 17.0, 10.2, 6.7 Hz, 1H), 5.01 – 4.95 (m, 1H), 4.92 (dq, J = 10.1, 1.5 Hz, 1H), 3.77 (q, J = 6.1 Hz, 1H), 2.07 – 2.00 (m, 2H), 1.88 (s, 1H), 1.49 – 1.26 (m, 10H), 1.17 (d, J = 6.3 Hz, 3H) ppm; ^{13}C NMR (151 MHz, $CDCl_3$) δ 139.2, 114.2, 68.1, 39.4, 33.8, 29.6, 29.2, 28.9, 25.8, 23.5 ppm.

1-(Allyloxy)propan-2-ol (9s, Figure 3) (Magre et al., 2020). The general procedure was followed. Colorless oil was isolated. Yield: 95 mg (82%). ^{1}H NMR (500 MHz, $CDCl_3$) δ 5.92 (ddt, J = 17.0, 10.2, 5.7 Hz, 1H), 5.29 (dd, J = 17.2, 1.6 Hz, 1H), 5.25 – 5.15 (m, 1H), 4.03 (dt, J = 5.7, 1.4 Hz, 2H), 3.98 (td, J = 6.3, 3.0 Hz, 1H), 3.44 (dd, J = 9.5, 3.0 Hz, 1H), 3.25 (dd, J = 9.5, 8.2 Hz, 1H), 2.55 (d, J = 2.7 Hz, 1H), 1.15 (d, J = 6.3 Hz, 3H) ppm; ^{13}C NMR (151 MHz, $CDCl_3$) δ 134.7, 117.3, 75.9, 72.3, 66.6, 18.8 ppm.

1-Methyl-4-(prop-1-en-2-yl)cyclohexan-1-ol (9t, Figure 3). The general procedure was followed. Colorless oil was isolated. Yield: 96 mg (62%). ^{1}H NMR (600 MHz, $CDCl_3$) δ 4.72 – 4.67 (m, 2H), 1.86 – 1.79 (m, 1H), 1.73 (s, 3H), 1.71 – 1.67 (m, 2H), 1.61 – 1.51 (m, 4H), 1.46 – 1.39 (m, 2H), 1.23 (s, 3H), 1.19 (s, 1H) ppm; ^{13}C NMR (151 MHz, $CDCl_3$) δ 150.5, 108.5, 69.0, 44.9, 39.0, 31.6, 27.2, 21.1 ppm. Elemental analysis calc. (%) for $C_{10}H_{18}O$: C 77.87, H 11.76; Found C 77.53, H 11.35.

3-Vinylcyclohexanol (9u, Figure 3) and 4-vinylcyclohexanol (9u′, Figure 3) (9u : 9u′ = 10:7) (Molander and McKie, 1992). The general procedure was followed. Colorless oil was isolated. Yield: 116 mg (92%). ^{1}H NMR (500 MHz, $CDCl_3$) δ 5.87 – 5.73 (m, overlapping, 1H), 5.04 – 4.90 (m, overlapping, 2H), 4.08 (br, 1H, **9u**), 3.95 (br, 1H, **9u′**), 2.46 (br, 1H, **9u**), 2.09 – 2.03 (m, 1H, **9u′**), 1.95 (s, overlapping, 1H), 1.78 – 1.49 (m, overlapping, 7H), 1.47 – 1.41 (m, 1H), 1.22 – 1.13 (m, 1H) ppm; ^{13}C NMR (151 MHz, $CDCl_3$) δ 143.8, 143.7, 112.6, 112.5, 66.9, 66.5, 40.0, 39.0, 35.6, 33.2, 32.1, 31.6, 26.7, 19.9 ppm.

1-(Prop-2-yn-1-yloxy)propan-2-ol (9v, Figure 3) (Steiniger and Lambert, 2021). The general procedure was followed. Colorless oil was isolated. Yield: 73 mg (64%). ^{1}H NMR (600 MHz, $CDCl_3$) δ 4.25 – 4.14 (m, 2H), 3.99 (ddt, J = 10.1, 6.2, 3.2 Hz, 1H), 3.54 (dd, J = 9.4, 3.2 Hz, 1H), 3.34 (dd, J = 9.5, 7.9 Hz, 1H), 2.55 (s, 1H), 2.47 (t, J = 2.5 Hz, 1H), 1.17 (d, J = 6.6 Hz, 3H) ppm; ^{13}C NMR (151 MHz, $CDCl_3$) δ 79.6, 75.6, 74.8, 66.4, 58.5, 18.8 ppm.

2-((1-Chloropropan-2-yl)oxy)-4,4,5,5-tetramethyl-1,3,2-dioxaborolane (9w, Figure 3). NMR yield: 99%. ^{1}H NMR (600 MHz, $CDCl_3$) δ 4.36 (td, J = 6.3, 5.3 Hz, 1H), 3.51 – 3.43 (m, 2H), 1.29 (d, J = 6.3 Hz, 3H), 1.26 (s, 12H) ppm; ^{13}C NMR (151 MHz, $CDCl_3$) δ 83.1, 70.7, 49.1, 24.7, 20.3 ppm. GC-MS: 220 (calc. 220).

2,2′-(Propane-1,2-diylbis(oxy))bis(4,4,5,5-tetramethyl-1,3,2-dioxaborolane) (9x, Figure 3) (Kobylarski et al., 2022). NMR yield: 94%. ^{1}H NMR (600 MHz, $CDCl_3$) δ 4.28 (q, J = 6.1 Hz, 1H), 3.75 (d, J = 5.6 Hz, 2H), 1.25 (s, 24H), 1.17 (d, J = 6.5 Hz, 3H) ppm; ^{13}C NMR (151 MHz, $CDCl_3$) δ 82.9, 82.7, 70.5, 69.3, 24.7, 18.7 ppm.

1,2-Diphenylethan-1-ol (9y, Figure 3) (Magre et al., 2020). White solid was isolated. Yield: 89 mg (45%). ^{1}H NMR (500 MHz, $CDCl_3$) δ 7.46 – 7.10 (m, 10H), 4.91 (ddd, J = 8.2, 4.8, 2.8 Hz, 1H), 3.08 – 2.97 (m, 2H), 1.94 (d, J = 3.0 Hz, 1H) ppm; ^{13}C NMR (101 MHz, $CDCl_3$) δ 144.0, 138.2, 129.7, 128.7, 128.6, 127.8, 126.8, 126.0, 46.3 ppm.

4,4,5,5-Tetramethyl-2-propoxy-1,3,2-dioxaborolane (10, Scheme S5) (Hadlington et al., 2014). NMR yield: 99%. ^{1}H NMR (500 MHz, $CDCl_3$) δ 3.75 (t, J = 6.6 Hz, 2H), 1.54 (dtd, J = 14.0, 7.4, 6.6 Hz, 2H), 1.21 (s, 12H), 0.87 (t, J = 7.4 Hz, 3H) ppm; ^{13}C NMR (126 MHz, $CDCl_3$) δ 82.5, 66.5, 24.5, 16.7, 10.0 ppm. GC-MS: 186 (calc. 186).

4,4,5,5-Tetramethyl-2-(phenyl(3-phenyloxiran-2-yl)methoxy)-1,3,2-dioxaborolane (11, Figure S7) (Zhang et al., 2022). ^{1}H NMR (500 MHz, $CDCl_3$) δ 7.53 – 7.45 (m, 2H), 7.38 (d, J = 7.8 Hz, 2H), 7.33 (dd, J = 7.2, 4.9 Hz, 3H), 7.31 – 7.25 (m, 3H), 5.30 (d, J = 3.6 Hz, 1H), 4.17 (d, J = 2.0 Hz, 1H), 3.23 (dd, J = 3.7, 2.0 Hz, 1H), 1.30 (d, J = 18.3 Hz, 13H) ppm; ^{13}C NMR (126 MHz, $CDCl_3$) δ 139.0, 137.0, 128.5, 128.4, 128.18, 128.15, 126.4, 125.8, 83.3, 74.1, 64.6, 55.4, 24.7, 24.5 ppm.

(R)-1-phenylethyl (R)-3,3,3-trifluoro-2-methoxy-2-phenylpropanoate (Hudlicky et al., 1991). ^{1}H NMR (600 MHz, $CDCl_3$) δ 7.34 (d, J = 7.7 Hz, 2H), 7.30 (t, J = 7.3 Hz, 1H), 7.23 (ddd, J = 17.5, 7.7, 5.6 Hz, 5H), 7.17 (dd, J = 7.4, 2.3 Hz, 2H), 6.02 (q, J = 6.6 Hz, 1H), 3.52 – 3.44 (m, 3H), 1.56 (d, J = 6.7 Hz, 3H) ppm; ^{13}C NMR (126 MHz, $CDCl_3$) δ 165.6, 140.2, 132.3, 129.5, 128.5, 128.3, 128.3, 127.3, 126.2, 124.5, 122.2, 84.6 (q, J = 27.7 Hz), 75.0, 55.49, 22.2 ppm.